On structural theories for ionic polymer metal composites: balancing between accuracy and simplicity

Alain Boldini · Lorenzo Bardella · Maurizio Porfiri

Received: date / Accepted: date

Abstract Ionic polymer metal composites (IPMCs) are soft electroactive materials that are finding increasing use as actuators in several engineering domains, where there is a need of large compliance and low activation voltage. Similar to traditional sandwich structures, an IPMC comprises a hydrated ionomer core that is sandwiched by two stiffer electrodes. The application of a voltage across the electrodes drives charge migration within the ionomer, which, in turn, contributes to the development of an eigenstress, associated with osmotic pressure and Maxwell stress. Critical to IPMC actuation is the variation of the eigenstress through the thickness of the ionomer, which is responsible for strain localization at the ionomer-electrode interfaces. Despite considerable progress in the development of reliable continuum theories and finite element tools, accurate structural theories that could beget physical insight into the inner workings of IPMC actuation are lacking. Here, we seek to bridge this gap by contributing a principled methodology to structural modeling of IPMC actuation. Our approach begins with the study of the IPMC electrochemistry through the method of matched asymptotic expansions, which yields a semi-analytical expression for the eigenstress as a function of the applied voltage. Hence, we establish a total potential energy that accounts for the strain energy of the ionomer, the strain energy of the electrodes, and the work performed by the eigenstress. By projecting the IPMC kinematics on select beam-like representation and imposing the stationarity of the total potential energy, we formulate rigorous structural theories for IPMC actuation. Not only do we examine classical low-order and higher-order beam theories, but we also propose enriched theories that account for strain localization near the electrodes. The accuracy of these theories is assessed through com-

A. Boldini

Department of Mechanical and Aerospace Engineering, Tandon School of Engineering, New York University, 6 MetroTech Center, Brooklyn, NY 11201, USA

L. Bardella

Department of Civil, Environmental, Architectural Engineering and Mathematics, University of Brescia, via Branze 43-45, 25123, Brescia, Italy

M. Porfiri (corresponding author)

Department of Mechanical and Aerospace Engineering and Department of Biomedical Engineering, Tandon School of Engineering, New York University, 6 MetroTech Center, Brooklyn, NY 11201, USA

Tel.: +1 646-997-3681 Fax: +1 646-997-3532 E-mail: mporfiri@nyu.edu

parison with finite element simulations on a plane-strain problem of non-uniform bending. Our results indicate that an enriched Euler-Bernoulli beam theory, with three independent field variables, is successful in capturing the main features of IPMC actuation at a limited computational cost.

Keywords Eigenstress \cdot Higher-order theories \cdot Multiaxial deformations \cdot Sandwich structures \cdot Through-the-thickness strains

1 Introduction

Since their invention more than two decades ago [1], ionic polymer metal composites (IPMCs) [2, 3] have attracted increasing consideration from scientists and engineers. Their relatively low driving voltage and large compliance compared to other electroactive materials are potential advantages for application as artificial muscles, in soft robotics [4, 5] and biomedical engineering [6]. The possibility of employing IPMCs in wet environments is another critical advantage, which has promoted enticing concepts in underwater robotics [7]. Recent developments in additive manufacturing of ionomer membranes [4, 8, 9] are expected to further extend the reach of these materials, allowing engineers to tailor IPMCs toward desired performance and motion patterns.

The most basic incarnation of IPMCs [1] consists of a sandwich-like structure, where a soft ionomer core is sandwiched by two stiffer electrodes [2, 3]. The ionomer core is typically a cation-exchange membrane, in which anions are fixed to the polymeric backbone, while cations are mobile within the solution that saturates the membrane. Different membrane types have been considered over the years, including NafionTM, FlemionTM, and Aquivion®, along with a range of imbuing solutions, from salt solutions to ionic liquids [10]. Due to their low resistivity, noble metals are commonly utilized as electrode materials [2, 3], although recent studies have explored the use of alternative solutions to reduce costs and improve durability and biological compatibility [11, 12, 13, 14].

The application of a voltage across the electrodes elicits the macroscopic bending of the actuator, mediated by complex microscopic electrochemical phenomena. Through the past two decades, several theories have been proposed to describe IPMC actuation [2, 3]. Since the seminal efforts in de Gennes et al. [15] and Nemat-Nasser and Li [16], charge redistribution in the ionomer has been identified as the main driver of actuation. Accompanying the migration of cations toward the cathode is the motion of the solvent molecules that is needed to maintain the electrochemical equilibrium. This motion generates a differential osmotic pressure near the electrodes, thereby causing a net bending moment toward the anode. This actuation mechanism is incorporated in most of the models of IPMC actuation, including cluster-based approaches tailored to IPMC physics [16] and continuum theories, grounded in linear irreversible thermodynamics [15], Poisson-Nernst-Planck equations [17, 18, 19, 20, 21, 22], mixtures [23], and porous media [24].

Despite the complexity of these modeling approaches, some peculiar IPMC phenomena have remained elusive for long. Particularly challenging was to explain the phenomenon of back-relaxation, which entails the surprising change in the direction of bending of an IPMC actuator under a constant applied voltage [25]. Several authors have attributed back-relaxation to the so-called added mass effect, whereby solvent molecules dragged during the counterions' migration will ultimately diffuse back to their original configuration, causing back-relaxation [26]. Due to some limitations of this hypothesis, our group has proposed an alternative explanation based on the nonlinear interplay of osmotic pressure and Maxwell

stress [27], showing qualitative agreement with experimental observations [28]. These predictions are anchored in a continuum theory of IPMC physics, encompassing both ion mixing and polarization effects [29]. This framework offers a powerful lens to study the inner workings of IPMCs, starting from first principles of thermodynamics, following the line of work by Hong et al. [30] for the study of polyelectrolytes.

Toward the simulation of the complete model in Cha and Porfiri [29], we have recently established a finite element (FE) solution for plane-strain deformations of IPMCs with zerothickness electrodes [31]. Specifically, we formulated a user-defined element (UEL) in the commercial FE software ABAQUSTM. Through FE simulations, we discovered that the two charged electrodes of an IPMC attract each other due to Maxwell stress like a capacitor, thereby causing a contraction along the thickness and a localized through-the-thickness strain in the vicinity of the electrodes. This strain component, absent in low-order structural models, modifies the effective axial stress of the ionomer, thereby drastically affecting its mechanical response. Building on these numerical results, we also derived a closed-form solution for uniform bending using the method of matched asymptotic expansions [32], which helps shed light on some of the numerical observations. However, this semi-analytical derivation [31] is limited to uniform bending, thereby preventing its use for general boundary conditions that may elicit a non-zero shear strain in the IPMC. FE simulations can address most boundary conditions with accuracy, but their computational cost is too high for design and optimization purposes. In addition to the hypothesis of uniform bending, the solution by Boldini and Porfiri [31] does not account for the presence of the electrodes, whose role on IPMC actuation is yet to be fully understood. Several studies in the field of composite structures have pointed at the critical role of stiff skins on bending of sandwich structures [33, 34]. Shear deformability in sandwich structures may play a significant role on shaping the overall mechanical deformation of the composite during non-uniform bending [33, 34, 35, 36, 37], and the presence of a soft core, where transverse deformations are significant, further exacerbates the complexity of the problem [38, 39, 40]. Within these structures, components of the in- and out-of-plane stress can display nontrivial profiles in the vicinity of the core-skin interfaces, with stress concentrations that depend on the ratios between the skins' and core Young moduli and thicknesses [37].

One possibility to bridge the versatility of FE simulations and the reduced computational cost of semi-analytical solutions is offered by structural theories. There is a long history of beam- and plate-like models for IPMC actuators [16, 26, 27, 29, 41]. Commonly used structural models rely on several assumptions, such as infinite rigidity of the cross-sections, which is in stark contrast with numerical simulations from our previous work [31]. Also, they assume independence between bending and extension, which is also in disagreement with our numerical observations that support a shift in the neutral axis during actuation. We should also mention that most of these models neglect the role of the electrodes on the deformation, beyond the mere scaling of the bending stiffness. Whether this assumption is accurate or not is presently unclear, whereby our numerical investigations were conducted under the premise of electrodes with zero thickness.

Several structural theories have been proposed in the literature to model sandwich structures. The simplest theories employ variants of Euler-Bernoulli or Timoshenko beam theories with rigidities homogenized over the entire cross-section [33, 42]. Higher-order shear deformation theories introduce warping to better capture deformability, for example through a "zig-zag" profile along the sandwich thickness [34, 36, 37]. To deal with transverse deformability of soft cores, more refined structural theories account for the through-the-thickness deformations in the core albeit retaining Euler-Bernoulli kinematics for thin skins [38, 43].

Alternative approaches have been recently proposed to study arbitrary material and geometric properties, combining key features of zig-zag and soft-core theories [39, 40].

While the theoretical framework of sandwich structures has never been applied to study IPMC actuation, a recent endeavor [44] has investigated how electrodes affect IPMC mechanics during sensing. Therein, the Krajcinovic sandwich theory [34], which relies on a zig-zag warping, was coupled with the theory in Cha and Porfiri [29] to examine the effect of IPMC shear deformation on sensing. This extension of Krajcinovic theory to IPMC sensing suggests that warping might be inherently coupled with IPMC electrochemistry. Hence, out-of-plane cross-section distortions should be expected in IPMC actuation as well, but, unlikely, existing theories will be able to capture the complexity of the nonlinear response underpinning IPMC actuation.

Here, we put forward a variational formulation to support the development of accurate structural theories of IPMC actuation. Toward this aim, we decouple electrochemistry from mechanics, such that IPMC actuation is summarized in an eigenstress that is computed once for all from the applied voltage. Following Boldini and Porfiri [31], this computation is carried out based upon the method of matched asymptotic expansions [17, 32]. To describe the mechanics of the IPMC, we introduce a total potential energy (TPE) [45], encompassing the strain energy of ionomer and electrodes, and work performed by the eigenstress. We specialize the approach to Euler-Bernoulli beam theory [46] and an enhanced high-order sandwich panel theory (EHOSPT) [43], accounting for the through-the-thickness deformability of the ionomer. To include the effect of localized, through-the-thickness strain in the vicinity of the ionomer-electrode interface, we enrich these theories with the through-the-thickness contraction associated with uniform bending, modulated by a function of the axial coordinate.

The stationarity of the total potential energy with kinematic constraints imposed by each model leads to a linear system of two-point boundary value problems (BVPs) with essential and natural boundary conditions. For the original and enriched Euler-Bernoulli beam theory, we present an exact derivation of the solution. On the other hand, for the original and enriched EHOSPT, we pursue a Fourier-series approach, similar to the classical approach of Pagano [47] in linear elasticity to find plane-strain solutions in composite plates with an arbitrary number of layers. The analysis of EHOSPT-based models is computationally more expensive than Euler-Bernoulli-based theories, since the former requires the solution of a large number of elementary linear systems (one for each harmonic), compared to the calculation of a few salient integrals associated with the eigenstress for the latter.

We compare the results of these structural models with nonlinear FE simulations in ABAQUSTM, utilizing a UEL to describe the mechanics and electrochemistry of the ionomer [31], with inert, linear elastic electrodes. In agreement with our expectations, the original Euler-Bernoulli beam theory has poor performance, whereby it fails to even capture the deflection profile. The original EHOSPT provides a better description of IPMC multiaxial deformations, as it is partially able to resolve the strain localization near the electrodes. However, its inability to accurately capture the localized thickness contraction significantly affects the reconstruction of displacements away from the IPMC mid-axis. On the other hand, the enriched versions of Euler-Bernoulli beam theory and EHOSPT afford the accurate resolution of the overall displacement, providing almost equivalent results in terms of deflections. The enriched EHOSPT displays a slightly better performance in the prediction of the through-the-thickness contraction of the IPMC, especially in the core of the ionomer, although it comes at a considerably larger computational cost. With respect to stresses, the enriched Euler-Bernoulli beam theory and enriched EHOSPT provide similar results, by accurately reproducing FE simulations.

The paper is organized as follows. Section 2 provides a review of the continuum model in Cha and Porfiri [29], under the hypothesis of small deformations, and results from the analysis of multiaxial deformations of IPMCs undergoing uniform bending [31]. In Section 3, we detail our approach to describe the mechanics and electrochemistry of IPMCs through reduced-order models. Therein, we introduce the TPE, present the structural models, and derive the governing equations associated with each model. Solutions of these structural models for specific boundary conditions leading to non-uniform bending and the comparison between these solutions and FE simulations are presented in Section 4. Section 5 concludes the paper and offers possible lines of future inquiry.

2 Background

The proposed approach to study IPMC actuation is anchored in the thermodynamically-consistent continuum theory proposed in Cha and Porfiri [29] to describe mechanics and electrochemistry of ionomers. Here, we briefly review the main aspects of the theory, which are combined with a structural model for the electrodes to establish our variational formulation for IPMC actuation. In principle, the theory is applicable to study both sensing and actuation in the presence of large deformations. However, we present the theory in a linearized form, where we neglect bidirectional coupling between mechanics and electrochemistry and we consider small deformations, while retaining nonlinearities in the electrochemistry. Such a linear treatment of IPMC mechanics is expected to be sufficient in practical applications, whereby IPMCs typically experience axial strains of less than 5% [48]. The FE analysis, instead, incorporates the complete nonlinear form of the theory from Cha and Porfiri [29].

Alongside the continuum theory [29], we review our previous analysis on multiaxial deformations in ionic membranes in plane-strain [31]. Specifically, we recall the main hypotheses of our semi-analytical solution, and outline its main results, which were previously validated through FE. The FE analysis, implemented in ABAQUSTM, is based on a UEL in plane-strain that allows for examining mechanics and electrochemistry of ionomers [31]. Here, this FE framework is adapted to study IPMC actuation by treating the electrodes as two isotropic, linear elastic layers.

2.1 Review of thermodynamically-consistent continuum theory

The continuum theory in [29] describes multiaxial deformations of cation-exchange ionic membranes, associated with bidirectional coupling between mechanics and electrochemistry. The ionomer consists of a negatively charged membrane, saturated and neutralized in a solution containing positive ions. Counterions can move through the membrane, and their migration is governed by diffusion and electromigration, following the application of a voltage across the electrodes. On the other hand, anions are fixed to the ionomer, and their concentration can only vary as a consequence of mechanical deformation.

Mechanics and electrochemistry of the ionomer are described with respect to the undeformed electroneutral configuration in which the point-wise mechanical stress, net charge, and electric potential are equal to zero. A point of the ionomer in the reference configuration is labelled as \mathbf{X} and t is the time variable. The three field variables of the theory are: the mechanical displacement, $\mathbf{u}(\mathbf{X},t)$; the counterions' concentration per unit undeformed volume, $C(\mathbf{X},t)$; and the voltage, $\psi(\mathbf{X},t)$ (with respect to a common ground).

Governing equations are obtained from conservation laws. Specifically, we consider the linear momentum balance for the ionomer, neglecting body forces and inertia, such that

$$Div \sigma = \mathbf{0}, \tag{1}$$

where σ is the, symmetric, Cauchy stress tensor and $Div(\cdot)$ indicates divergence. We assume that no chemical reaction occurs in the ionomer and at the interface with the electrodes, such that counterions' concentration is conserved,

$$\frac{\partial C}{\partial t} + \text{Div } \mathbf{J} = 0, \tag{2}$$

where **J** is the counterions' flux. Electrodynamics is neglected, so that the electric field **E** is irrotational and we define a scalar electric potential ψ such that $\mathbf{E} = -\nabla \psi$, where $\nabla(\cdot)$ indicates the gradient. In this framework, the last governing equation of the model is Gauss law, namely,

$$Div \mathbf{D} = Q, \tag{3}$$

where **D** is the electric displacement, and

$$Q = \mathcal{F}(C - C_0) \tag{4}$$

is the net charge per unit undeformed volume. Here, $\mathscr{F} = 96,485\,\mathrm{C\,mol}^{-1}$ is the Faraday constant, while C_0 represents the concentration per unit undeformed volume of fixed ions in the membrane. In the following, we hypothesize that C_0 is homogeneous in the membrane.

The system of partial differential equations (PDEs) in Eqs. (1), (2), and (3) must be complemented by constitutive equations describing the mechanical and electrochemical response of the material. In Cha and Porfiri [29], nonlinear constitutive laws are obtained through a thermodynamically-consistent approach, based on the definition of a free-energy density, encompassing the strain energy of the ionomer, and the free-energy associated with ion mixing and polarization. By suitably differentiating the free-energy, one can obtain constitutive laws that satisfy the second principle of thermodynamics. Here, we specialize the constitutive equations derived in Cha and Porfiri [29] to the case of small deformations, also neglecting steric effects and bidirectional coupling between sensing and actuation that were considered therein. The Cauchy stress tensor in Eq. (1) can be written as

$$\sigma = \sigma_{\text{mec}} + \sigma_{\text{ion}} + \sigma_{\text{pol}} \tag{5}$$

where σ_{mec} is the mechanical stress in the ionomer, σ_{ion} is the osmotic pressure generated by charge gradients [30], and σ_{pol} is Maxwell stress due to electric polarization [49]. Osmotic effects and Maxwell stress constitute the eigenstress in the ionomer, which we consolidate into

$$\sigma_0 = \sigma_{\text{ion}} + \sigma_{\text{pol}}. \tag{6}$$

Assuming that the ionomer is isotropic, the mechanical stress σ_{mec} is

$$\sigma_{\rm mec} = \lambda_{\rm L} \operatorname{tr}(\varepsilon) \mathbf{I} + 2\mu_{\rm L} \varepsilon, \tag{7}$$

where

$$\varepsilon = \frac{1}{2} (\nabla \mathbf{u} + \nabla \mathbf{u}^{\mathrm{T}}) \tag{8}$$

is the infinitesimal strain tensor, T indicates transposition, I is the identity tensor, $tr(\cdot)$ represents the trace operator, and λ_L and μ_L are the Lamé parameters for the ionomer. In the

complete FE analysis, a Saint Venant-Kirchhoff model is implemented [29]. When modeling ion mixing, we assume a dilute solution [50], such that

$$\sigma_{\text{ion}} = -\Re \mathcal{T}(C - C_0)\mathbf{I},\tag{9}$$

where $\mathcal{R} = 8.314 \text{J} \, \text{mol}^{-1} \, \text{K}^{-1}$ is the universal gas constant and \mathcal{T} is the absolute temperature. This spherical tensor encapsulates the effect of the osmotic pressure, which grows proportionally to the charge imbalance. Finally, we assume that the material is dielectrically isotropic, such that Maxwell stress tensor [49] is given by

$$\sigma_{pol} = \frac{1}{\varepsilon} \left[\mathbf{D} \otimes \mathbf{D} - \frac{1}{2} (\mathbf{D} \cdot \mathbf{D}) \mathbf{I} \right], \tag{10}$$

where ε is the dielectric constant of the ionomer, " \otimes " indicates the tensor product, and " \cdot " is the inner product. We assume that ε is constant in the ionomer.

When considering electrochemical constitutive equations, the dielectric isotropy of the material implies [49]

$$\mathbf{E} = \frac{1}{\varepsilon} \mathbf{D},\tag{11}$$

and the diluteness of the solution leads to the following form of the electrochemical potential μ [50]:

$$\mu = \mathcal{F}\psi + \mathcal{R}\mathcal{T}\ln\frac{C}{C_0}.$$
 (12)

Finally, we implement the classical Nernst-Planck linear constitutive law for the flux of chemical species [50], that is,

$$\mathbf{J} = -\frac{\mathscr{D}C}{\mathscr{R}\mathscr{T}}\nabla\mu,\tag{13}$$

where \mathcal{D} is the diffusivity of counterions in the membrane. In the complete FE analysis, both the electrochemical potential and the flux account for the effect of mechanical deformation, which is neglected in this linearized model.

Boundary conditions must be specified at the interface with either the electrodes (\mathcal{S}_{el}) or the surrounding environment (\mathcal{S}_{ext}), including air or water depending on the application. For simplicity, we suppose that the electrodes are perfect, that is, their resistivity is negligible and they are ion-blocking. The former hypothesis allows us to neglect voltage drops across and along the electrodes, such that the electric potential at the interface is equal to the uniform potential \bar{V} of the electrode,

$$\psi = \bar{V} \quad \text{on } \mathcal{S}_{el}.$$
(14)

The value of this voltage is imposed externally during actuation, while it is determined by mechanical deformation during sensing. The validity of this hypothesis may be strained when considering relatively long IPMCs, where significant voltage attenuation along the electrodes may be observed [51]. The ion-blocking hypothesis implies

$$\mathbf{J} \cdot \mathbf{N} = 0 \quad \text{on } \mathcal{S}_{el}, \tag{15}$$

where N is the normal to the surface \mathscr{S}_{el} in the reference configuration.

At the interface with the surrounding environment, we assume that there is no counterions' flux through the surface and that the normal component of the electric displacement is zero to avoid loss of charges, such that

$$\mathbf{J} \cdot \mathbf{N} = 0 \quad \text{on } \mathcal{S}_{\text{ext}}, \tag{16a}$$

$$\mathbf{D} \cdot \mathbf{N} = 0 \quad \text{on } \mathcal{S}_{\text{ext}}. \tag{16b}$$

We expect these boundary conditions to be reasonably satisfied for IPMCs in air or deionized water.

In light of our assumptions, electrodes play a role exclusively on shaping the mechanical response of the IPMC, whereby the voltage is constant therein and ions concentrations are zero. We suppose that the electrodes follow a linear elastic behavior, for which we specify electrodes' Young modulus $Y_{\rm el}$ and Poisson ratio $V_{\rm el}$.

2.2 Semi-analytical solution for uniform bending and zero-thickness electrodes

Our effort to develop viable structural theories for IPMCs is grounded in our previous investigation of multiaxial deformations [31], which evidenced a critical role of through-the-thickness deformation in the vicinity of the electrodes in shaping the macroscopic response. Therein, we proposed a semi-analytical solution for plane-strain deformations of IPMCs with zero-thickness electrodes, in the case of uniform bending. Such a solution was validated through FE simulations of the continuum theory summarized above, in the complete nonlinear form presented in Cha and Porfiri [29]. The same FE formulation, with the addition of electrodes, is utilized in the following as ground truth to assess the accuracy of the proposed structural theories.

Throughout the paper, we consider a rectangular IPMC of length l, with an ionomer core of thickness $2h \ll l$ and two electrodes of the same thickness $e \ll h$, under plane-strain conditions. We consider a reference frame at the center of the ionomer thickness at the left end of the ionomer, with the X-axis along the axis of the IPMC, Y-axis pointing through its thickness toward the anode, and Z-axis along its width (Fig. 1).

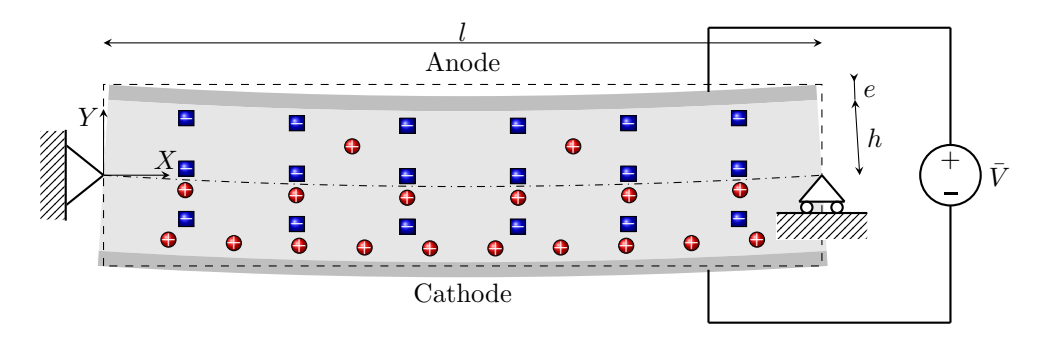


Fig. 1 Schematics of IPMC actuation, with simply supporting boundary conditions. Upon the application of an external voltage across its electrodes, counterions (in red) migrate toward the cathode, while anions (in blue) are fixed to the ionomer membrane.

For simplicity, the interface between the ionomer and the electrodes is assumed to be flat in the undeformed configuration. While this hypothesis may be valid macroscopically, the roughness of the interface at a microscopic level plays a fundamental role on the impedance of the IPMC, whereby it provides a capacitance-boost that considerably enhances IPMC actuation [52, 53]. This effect may be considered by introducing composite layers with a

different dielectric constant near the interface, to mimic the increase of effective surface area associated with the rough landspace of the interface [54].

In Boldini and Porfiri [31], we put forward two critical simplifying hypotheses, which will be relaxed in the following Section. Specifically, we assume that the IPMC is simply supported along its mid-axis, and that electrodes have zero thickness, that is, we set e=0. In light of the first hypothesis, we can neglect shear stresses in the IPMC, which undergoes uniform bending. Hence, we can decouple the through-the-thickness equilibrium from the equilibrium along the axial direction and we solve the former to obtain the through-the-thickness strain. This result is, in turn, utilized in the equilibrium along the axial direction to determine the effective axial stress. By following this procedure, we can obtain a semi-analytical solution for the mechanical deformation. The hypothesis of zero-thickness electrodes allows us to neglect the presence of the electrodes in any of these computations. However, the validity of this hypothesis might be questionable, based on overwhelming evidence in the field of composite structures [33, 34, 37, 38], which has highlighted how stiff skins in a three-layered sandwich could drastically affect the deformation of the structure.

The semi-analytical solution for multiaxial deformations of ionomer membranes in plane-strain [31] is based on a Saint-Venant approach that is valid away from the edges of the IPMC. First, we solve the nonlinear electrochemistry through the thickness of the ionomer, which is independent of the mechanical deformation and can be computed a-priori given the voltage applied across the electrodes. A solution of the resulting system of PDEs, commonly known as Poisson-Nernst-Planck (PNP) system [17, 50, 55], is obtained through the method of matched asymptotic expansions. In practice, we determine the nondimensional voltage drop α , defined with respect to the thermal voltage $V_{\rm th} = \Re \mathcal{T}/\mathcal{F}$, across the boundary layers near the electrodes by solving a simple ordinary differential equation (ODE) of a circuit model. From the ODE solution, we recover the profiles of counterions' concentration and voltage through the thickness of the ionomer. Details of the procedure are provided in A.

Once the through-the-thickness electrochemical profiles have been computed through the method of matched asymptotic expansions, we can evaluate the eigenstress related to osmotic pressure and Maxwell stress. We substitute the counterions' concentration and voltage along the thickness from Eq. (87) into Eqs. (9) and (10). Thus, the components of the eigenstress in Eq. (6) read

$$\sigma_{0_{XX}}(Y) = \sigma_{0_{ZZ}}(Y) = -\Re \mathscr{T}(C(Y) - C_0) - \frac{\varepsilon}{2} \left(\frac{\partial \psi(Y)}{\partial Y}\right)^2, \tag{17a}$$

$$\sigma_{0\gamma\gamma}(Y) = -\Re \mathscr{T}(C(Y) - C_0) + \frac{\varepsilon}{2} \left(\frac{\partial \psi(Y)}{\partial Y}\right)^2,$$
 (17b)

$$\sigma_{0_{XY}}(Y) = \sigma_{0_{XZ}}(Y) = \sigma_{0_{YZ}}(Y) = 0.$$
 (17c)

Here and henceforth, we omit the dependence on time for the sake of legibility.

In addition, under plane-strain the sole non-vanishing components of the strain tensor are

$$\varepsilon_{XX}(X,Y) = \frac{\partial u(X,Y)}{\partial X},$$
 (18a)

$$\varepsilon_{YY}(X,Y) = \frac{\partial w(X,Y)}{\partial Y},$$
 (18b)

$$\varepsilon_{XY}(X,Y) = \frac{1}{2} \left(\frac{\partial u(X,Y)}{\partial Y} + \frac{\partial w(X,Y)}{\partial X} \right),$$
 (18c)

where u(X,Y) and w(X,Y) are the longitudinal and transverse displacements.

Mirroring the treatment of electrochemistry (see A), we neglect variations of the strain along the IPMC axis and width. Therefore, the overall stress in the ionomer is

$$\sigma_{XX}(Y) = (\lambda_{L} + 2\mu_{L})\varepsilon_{XX}(Y) + \lambda_{L}\varepsilon_{YY}(Y) + \sigma_{0_{YY}}(Y), \tag{19a}$$

$$\sigma_{YY}(Y) = \lambda_{L} \varepsilon_{XX}(Y) + (\lambda_{L} + 2\mu_{L}) \varepsilon_{YY}(Y) + \sigma_{0vv}(Y), \tag{19b}$$

$$\sigma_{XY}(Y) = 2\mu_{L}\varepsilon_{XY}(Y). \tag{19c}$$

Inspired by the Saint-Venant solution for uniform bending with eccentricity, we assume a linear form of the axial strain

$$\varepsilon_{XX}(Y) = -kY + \varepsilon_0, \tag{20}$$

where k and ε_0 are the curvature and mid-axis strain of the ionomer, respectively, while neglecting the shear strain $\varepsilon_{XY}(Y)$. From equilibrium and stress-free boundary conditions, we find that the through-the-thickness stress in Eq. (19b) is point-wise zero along the thickness of the ionomer. This condition provides an equation for the through-the-thickness strain $\varepsilon_{YY}(Y)$, namely,

$$\varepsilon_{YY}(Y) = -\frac{1}{\lambda_{I} + 2\mu_{I}} \left[\lambda_{L} \varepsilon_{XX}(Y) + \sigma_{0_{YY}}(Y) \right], \tag{21}$$

which presents a non-trivial dependence on the through-the-thickness coordinate Y, where we observe strain boundary layers at the interface with the electrodes. For the parameters in Tab. 1, corresponding to a Young modulus for the ionomer $\left(Y_i = \frac{\mu_L(3\lambda_L + 2\mu_L)}{\lambda_L + \mu_L}\right)$ of 150 MPa and a Poisson ratio $\left(v_i = \frac{\lambda_L}{2(\lambda_L + \mu_L)}\right)$ of 0.45, we display strain localization in Fig. 2.

Parameter	Value
$\mathscr{T}[K]$	300
$C_0 [\mathrm{mol}\mathrm{m}^{-3}]$	1200
$\mathscr{D}[\mathrm{m}^2\mathrm{s}^{-1}]$	1×10^{-11}
$\varepsilon [\mathrm{Fm}^{-1}]$	4.48×10^{-5}
$h[\mu m]$	100
l [mm]	2
$\lambda_{\rm L} [{ m Pa}]$	4.6552×10^{8}
$\mu_{\rm L} [{\rm Pa}]$	5.1724×10^{7}

Table 1 Parameters utilized in the simulations, borrowed from Boldini and Porfiri [31].

The non-zero through-the-thickness strain from Eq. (21) elicits a contraction of the ionomer thickness. Similar to a capacitor, the accumulation of charges in the vicinity of the electrodes generates Maxwell stress, such that the electrodes will be attracted by each other. We quantify this contraction point-wise along the ionomer thickness by defining the displacement with respect to the IPMC mid-axis, namely,

$$\bar{f}(Y) = \int_{0}^{Y} \varepsilon_{YY}(\tilde{Y}) \, d\tilde{Y}. \tag{22}$$

Such a thickness contraction plays a significant role in determining the ionomer response, challenging the adoption of classical structural theories that rely on the infinite transveral rigidity of cross-sections, such as Euler-Bernoulli and Timoshenko beam theories [46]. Note

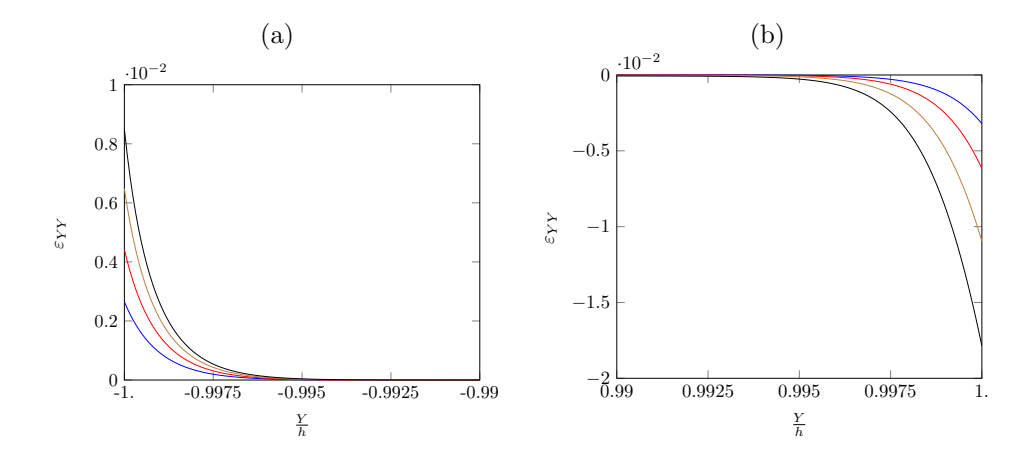


Fig. 2 Through-the-thickness strain in the vicinity of the cathode (a) and anode (b), for a step voltage $\bar{V} = 5V_{\rm th}$, at time t = 0.25 s (blue line), t = 0.5 s (red line), t = 1 s (brown line), and t = 7.5 s (black line) for the material constants in Tab. 1. Results are computed from the semi-analytical model in [31]. We note that the strains are not self-similar, since scaling the strain by the peak value at the interface will lead to different profiles, especially toward the anode.

that we had omitted the time dependence for the purpose of improved legibility, but the function in Eq. (22) evolves with time as well.

By substituting the axial and through-the-thickness strains $\varepsilon_{XX}(Y)$ and $\varepsilon_{YY}(Y)$ from Eqs. (20) and (21) in Eq. (19a), we find that the axial stress is completely determined by the knowledge of the mid-axis strain ε_0 of the ionomer, its curvature k, and the electrochemical variables, known from matched asymptotic expansions. Expressions for the ionomer mid-axis strain and its curvature can be found by computing the resultant axial force and bending moment, which must be equal to zero as no external force is applied on the ionomer.

Specifically, we obtain [31]

$$\varepsilon_0 = \frac{\mathscr{R}\mathscr{T}C_0}{8\mu_{\rm L}}\delta\mathscr{H}(\alpha),\tag{23a}$$

$$\beta k + M_{\text{ion}} + M_{\text{pol}} = 0, \tag{23b}$$

where β , $M_{\rm ion}$, and $M_{\rm pol}$ are the bending stiffness, bending moment associated with osmotic pressure, and bending moment related to Maxwell stress, respectively, whose expression is given by [31]

$$\beta = \frac{8}{3}\mu_{L}\frac{\lambda_{L} + \mu_{L}}{\lambda_{L} + 2\mu_{L}}h^{3},\tag{24a}$$

$$M_{\rm ion} = -4\mathscr{R}\mathscr{T}C_0h^2\frac{\mu_{\rm L}}{\lambda_{\rm L} + 2\mu_{\rm L}}\delta\vartheta(\alpha), \tag{24b}$$

$$M_{\rm pol} = 2\mathscr{R}\mathscr{T}C_0h^2\frac{\lambda_{\rm L} + \mu_{\rm L}}{\lambda_{\rm L} + 2\mu_{\rm L}}\delta\mathscr{G}(\alpha). \tag{24c}$$

In these expressions, $\delta = \frac{1}{\mathscr{F}h} \sqrt{\frac{\varepsilon \mathscr{R}\mathscr{T}}{C_0}}$ is the ratio between the Debye screening length λ [17, 50] and the semi-thickness h of the ionomer membrane, while $\mathscr{H}(\alpha)$, $\vartheta(\alpha)$, and $\mathscr{G}(\alpha)$

are universal functions, common to all IPMCs, whose full expressions and polynomial fits can be found in Boldini and Porfiri [31].

From the fact that $\mathcal{H}(\alpha) \geq 0$ and Eq. (23a), we conclude that the ionomer membrane is subject to an overall elongation along its axis. In Boldini and Porfiri [31], we demonstrated that such an elongation is coupled to the through-the-thickness contraction, such that the overall deformation is volume-preserving, regardless of the value of the Poisson ratio.

Despite the deep insight in multiaxial deformations provided by this exact solution, its range of applicability is limited. In fact, our treatment [31] does not account for the electrodes, which are expected to play a critical role in determining the overall axial and bending stiffness of the IPMC. Similar to previous endeavours in the literature of composite structures [33, 34, 37, 38], electrodes may cause qualitative differences in the response of IPMCs, with stress concentrations at the ionomer-electrode interfaces during bending that would overlap with the stress concentrations already induced by the eigenstress. In addition, the proposed solution is restricted to uniform bending, where shear deformations are negligible. The chief goal of this paper is to develop structural theories that can accurately describe multiaxial deformations in IPMCs, for general boundary conditions and electrodes with nonzero thickness.

3 Variational formulation based on structural theories

In this Section, we relax the hypotheses of uniform bending and zero-thickness electrodes that were adopted in Boldini and Porfiri [31]. By accounting for arbitrary boundary conditions and the presence of the electrodes, the determination of a semi-analytical solution for multiaxial mechanical deformations becomes substantially unfeasible. To address this issue, we formulate a TPE [45], upon which we establish structural theories for IPMC actuation.

Our approach to describe the mechanics and electrochemistry of IPMCs unfolds along the following steps. First, we study the electrochemistry through the thickness of the IPMC, in the form of a one-dimensional (1D) nonlinear system of PDEs. The problem is solved through the matched asymptotic expansions method [32], which allows for computing the counterions' concentration and voltage profiles through the thickness at any time instant t, independent of the mechanical deformation. From the counterions' concentration and voltage, we compute the eigenstress associated with osmotic pressure and Maxwell stress. Since we consider inert electrodes that do not affect the electrochemistry in the ionomer, this step is identical to the treatment in Boldini and Porfiri [31], which is briefly summarized in A.

To compute the mechanical deformation from the eigenstress, we first define a TPE [45], encompassing the strain energy of the ionomer and electrodes and the work done by the eigenstress. We introduce four different structural models to describe the kinematics of ionomer and electrodes. We consider two classical approaches from the literature, that is, Euler-Bernoulli beam theory¹ [46] and EHOSPT [43]. In addition, we propose two extensions of these models that include the through-the-thickness contraction, in Eq. (22), arising from uniform bending [31]. To accommodate different boundary conditions, we assume that the contraction in the enriched models is modulated by a function of the axial coordinate, which acts as an additional field variable. By substituting these kinematic relationships in the TPE and imposing its stationarity, we obtain BVPs for each degree of freedom present in the structural theory.

Strictly speaking, one should refer to this theory as Kirchhoff-Love plate theory for cylindrical bending, given the underlying plane-strain assumptions.

We consider again the sample problem in Fig. 1, consisting of a rectangular IPMC that is initially electroneutral and stress-free. We hypothesize that electrodes are thin ($e \ll h \ll l$), but with finite thickness, and we consider more general boundary conditions. Within this framework, matching conditions at the interface between the ionomer and the electrodes include the continuity of the longitudinal and transverse displacements, and normal and tangential stresses, that is,

$$u^{\text{el}^{\pm}}(X, \pm h) = u^{\text{i}}(X, \pm h),$$
 (25a)

$$w^{\text{el}^{\pm}}(X, \pm h) = w^{\text{i}}(X, \pm h),$$
 (25b)

$$\sigma_{YY}^{\text{el}^{\pm}}(X, \pm h) = \sigma_{YY}^{\text{i}}(X, \pm h), \tag{25c}$$

$$\sigma_{YY}^{\text{el}^{\pm}}(X,\pm h) = \sigma_{YY}^{\text{i}}(X,\pm h), \tag{25d}$$

where apices "i", "el+" and "el-" indicate the ionomer, anode, and cathode regions, respectively.

3.1 Total potential energy

We partition the TPE per unit width, U, into three contributions,

$$U = U_{\text{mec}} + U_{\text{el}} + \mathcal{W}_{\text{eig}}, \tag{26}$$

where U_{mec} and U_{el} are the strain energies per unit width associated with the ionomer and the electrodes, respectively, and W_{eig} is the work per unit width done by the eigenstress.

The strain energy of the ionomer is given by the integration of the free-energy density $W_{\text{mec}} = \frac{1}{2}\sigma_{\text{mec}} \cdot \varepsilon$ on the X-Y plane \mathscr{S}^i of the ionomer. Within the hypothesis of planestrain, Eq. (7) implies

$$U_{\text{mec}} = \int_{\mathscr{S}^{i}} W_{\text{mec}} dS = \frac{1}{2} \int_{\mathscr{S}^{i}} \left[(\lambda_{\text{L}} + 2\mu_{\text{L}}) \left[(\varepsilon_{XX}^{i})^{2} + (\varepsilon_{YY}^{i})^{2} \right] + 2\lambda_{\text{L}} \varepsilon_{XX}^{i} \varepsilon_{YY}^{i} + \mu_{\text{L}} (\gamma_{XY}^{i})^{2} \right] dS, \tag{27}$$

where $\gamma_{XY}^{i} = 2\varepsilon_{XY}^{i}$ is the shear strain in the ionomer.

Following standard practice in the literature on composite structures [33, 38], we treat the thin electrodes as Euler-Bernoulli beams. Specifically, we assume that, for any structural model, the displacement of the electrodes has the form

$$u^{\mathrm{el}^{\pm}}(X,Y) = u_0^{\mathrm{el}^{\pm}}(X) - \left[Y \mp \left(h + \frac{e}{2}\right)\right] \frac{\partial w_0^{\mathrm{el}^{\pm}}(X)}{\partial X},\tag{28a}$$

$$w^{\text{el}^{\pm}}(X,Y) = w_0^{\text{el}^{\pm}}(X),$$
 (28b)

where $u_0^{\mathrm{el}^+}(X), u_0^{\mathrm{el}^-}(X), w_0^{\mathrm{el}^+}(X)$, and $w_0^{\mathrm{el}^-}(X)$ are the mid-axis longitudinal displacement of the anode and cathode and the mid-axis transverse displacement of the anode and cathode, respectively. Therefore, the overall strain energy of the electrodes is given by

$$U_{\rm el} = \frac{1}{2} \int_{\mathscr{C}^{\rm el^{+}}} Y'_{\rm el} \left(\varepsilon_{XX}^{\rm el^{+}} \right)^{2} dS + \frac{1}{2} \int_{\mathscr{C}^{\rm el^{-}}} Y'_{\rm el} \left(\varepsilon_{XX}^{\rm el^{-}} \right)^{2} dS, \tag{29}$$

where \mathscr{S}^{el^+} and \mathscr{S}^{el^+} indicate the domains of the anode and cathode, respectively, and from Eqs. (18) and (28),

$$\varepsilon_{XX}^{\mathrm{el}^{\pm}}(X,Y) = \frac{\partial u^{\mathrm{el}^{\pm}}(X,Y)}{\partial X} = \frac{\partial u_{0}^{\mathrm{el}^{\pm}}(X)}{\partial X} - \left[Y \mp \left(h + \frac{e}{2}\right)\right] \frac{\partial^{2} w_{0}^{\mathrm{el}^{\pm}}(X)}{\partial X^{2}}.$$
 (30)

We recall that, for plane-strain, the Young modulus $Y_{\rm el}$ of the electrodes should be substituted by the effective Young modulus $Y_{\rm el}'$ [56], that is, $Y_{\rm el}' = Y_{\rm el}/(1-v_{\rm el}^2)$, where $v_{\rm el}$ is the Poisson ratio of the electrodes. As only four variables are required to describe the electrodes' displacement field, that is, $u_0^{\rm el}$ and $w_0^{\rm el}$, we can always obtain the kinematics of the electrodes as a function of the kinematics of the ionomer, by utilizing the four matching conditions for longitudinal and transverse displacements in Eq. (25).

Finally, the work performed by the eigenstress is given by

$$\mathcal{W}_{\text{eig}} = \int_{\mathcal{S}^{i}} (\sigma_{0} \cdot \varepsilon^{i}) \, dS = \int_{\mathcal{S}^{i}} \left(\sigma_{0_{XX}} \varepsilon_{XX}^{i} + \sigma_{0_{YY}} \varepsilon_{YY}^{i} \right) dS. \tag{31}$$

Here, the eigenstress is equal to Eq. (17), with the counterions' concentration and voltage a-priori determined from the matched asymptotic expansions (A).

3.2 Structural theories

In the following, we present four structural theories that can be adopted to describe IPMC multiaxial deformations. Two of them are based on classical beam theory: the simplest is Euler-Bernoulli beam theory [46], which describes the ionomer deformation through the longitudinal and transverse displacements of its mid-axis, while the more complex model entails EHOSPT, a higher-order theory that accounts for transverse deformability of the ionomer [43]. The other two theories are enrichments that account for localized through-the-thickness deformation at the electrode-ionomer interface. Inspired by classical treatments of shear deformations in Saint-Venant problems [56], we superimpose the through-the-thickness strain obtained from uniform bending to the transverse displacement of the original structural theories. Since boundary conditions could affect the through-the-thickness contraction, we modulate the deformation from uniform bending with an unknown function p(X) of the axial coordinate X.

3.2.1 Original and enriched Euler-Bernoulli beam theories

Within the classical framework of Euler-Bernoulli beam theory [46], the displacement field in the ionomer is determined by the mid-axis longitudinal and transverse displacements $(u_0^i(X))$ and $w_0^i(X)$, respectively), such that

$$u^{i}(X,Y) = u_{0}^{i}(X) - Yw_{0X}^{i}(X),$$
 (32a)

$$w^{i}(X,Y) = w_{0}^{i}(X).$$
 (32b)

Here and henceforth, we indicate derivatives at the pedices, while omitting the explicit dependence on time.

The simple kinematic assumptions of the original Euler-Bernoulli beam theory in Eq. (32) beget a non-zero axial strain with null shear and through-the-thickness strains. These simplistic assumptions are likely to lead to inadequate predictions of IPMC actuation, based on the results summarized in Section 2.2.

In order to describe through-the-thickness contraction of the ionomer, we propose an enriched Euler-Bernoulli beam theory with strain localization at the ionomer-electrodes interfaces. In particular, we add through-the-thickness non-uniform transverse component of the displacement in the ionomer in Eq. (32b). This deformation is described through a new field variable p(X), which modulates the function $\bar{f}(Y)$ in Eq. (22); for electrodes with

zero-thickness and uniform bending, this field variable is equal to one along the IPMC span. Hence, the kinematics of the enriched Euler-Bernoulli beam theory is

$$u^{i}(X,Y) = u_{0}^{i}(X) - Yw_{0,X}^{i}(X),$$
 (33a)

$$w^{i}(X,Y) = w_{0}^{i}(X) + p(X)\bar{f}(Y),$$
 (33b)

with the corresponding strains from Eq. (18),

$$\varepsilon_{XX}^{i}(X,Y) = u_{0,X}^{i}(X) - Yw_{0,XX}^{i}(X),$$
 (34a)

$$\varepsilon_{YY}^{i}(X,Y) = p(X)\bar{f}_{,Y}(Y), \tag{34b}$$

$$\gamma_{XY}^{\mathbf{i}}(X,Y) = p_X(X)\bar{f}(Y). \tag{34c}$$

We only provide the derivation for this enriched Euler-Bernoulli beam theory, whereby we can recover the original one by setting $\bar{f}(Y) = 0$.

The introduction of a function depending on *Y* in the transverse displacement of the ionomer yields non-zero through-the-thickness strain and non-zero shear strain, associated with the variation of the through-the-thickness contraction along the axis of the IPMC. Both effects are expected to play an important role when dealing with IPMC with electrodes of non-zero thickness and more general boundary conditions. For example, when testing IPMC for their blocked force [2], one is clamping one side of the actuator and pinning the other one with a load cell, thereby triggering shear deformations along with through-the-thickness contraction.

By imposing the matching conditions in Eq. (25), the electrodes' displacement in Eq. (33) is obtained as a function of the displacement of the ionomer in Eq. (32),

$$u^{\text{el}^{\pm}}(X,Y) = u_0^{\text{i}}(X) - Yw_{0,Y}^{\text{i}}(X) - (Y \mp h)p_X(X)\bar{f}(\pm h), \tag{35a}$$

$$w^{\text{el}^{\pm}}(X,Y) = w_0^{\text{i}}(X) + p(X)\bar{f}(\pm h),$$
 (35b)

such that from Eq. (18) the axial strain in the electrodes is

$$\varepsilon_{XX}^{\text{el}^{\pm}}(X,Y) = u_{0X}^{\text{i}}(X) - Y w_{0XX}^{\text{i}}(X) - (Y \mp h) p_{XX}(X) \bar{f}(\pm h). \tag{36}$$

Predictably, the longitudinal displacement of the electrodes in Eq. (35a) mirrors that of the ionomer in Eq. (32a), with an additional term related to the rotation of the electrodes in the case of non-uniform through-the-thickness contraction along the IPMC axis.

We substitute Eqs. (34) and (36) in the TPE contributions, that is, Eqs. (27), (29), and (31), and perform integrations along the thickness of the ionomer and electrodes, such that

the TPE reads

$$\begin{split} U &= \left[(\lambda_{L} + 2\mu_{L})h + Y_{el}'e \right] \int_{0}^{l} \left(u_{0,X}^{i} \right)^{2} dX \\ &+ \frac{h^{3}}{3} \left\{ (\lambda_{L} + 2\mu_{L}) + Y_{el}' \left[\left(1 + \frac{e}{h} \right)^{3} - 1 \right] \right\} \int_{0}^{l} \left(w_{0,XX}^{i} \right)^{2} dX \\ &+ \frac{1}{2} (\lambda_{L} + 2\mu_{L}) \mathscr{I}_{Y} ((\bar{f},Y)^{2}) \int_{0}^{l} p^{2} dX + \lambda_{L} \left[\mathscr{I}_{Y} (\bar{f},Y) \int_{0}^{l} p u_{0,X}^{i} dX - \mathscr{I}_{Y} (\bar{f},YY) \int_{0}^{l} p w_{0,XX}^{i} dX \right] \\ &+ \frac{1}{2} \mu_{L} \int_{0}^{l} (p_{,X})^{2} \mathscr{I}_{Y} (\bar{f}^{2}) dX \\ &+ \frac{1}{2} Y_{el}'e^{2} \left\{ \frac{e}{3} \left[(\bar{f}(h))^{2} + (\bar{f}(-h))^{2} \right] \int_{0}^{l} (p_{,XX})^{2} dX - \mathscr{I}_{Y} (\bar{f},Y) \int_{0}^{l} u_{0,X}^{i} p_{,XX} dX \right. \\ &+ \left. \left(h + \frac{2}{3} e \right) \left[\bar{f}(h) + \bar{f}(-h) \right] \int_{0}^{l} p_{,XX} w_{0,XX}^{i} dX \right\} + \mathscr{I}_{Y} (\sigma_{0_{XX}}) \int_{0}^{l} u_{0,X}^{i} dX \\ &- \mathscr{I}_{Y} (\sigma_{0_{XX}} Y) \int_{0}^{l} w_{0,XX}^{i} dX + \mathscr{I}_{Y} (\sigma_{0_{YY}} \bar{f},Y) \int_{0}^{l} p dX, \end{split} \tag{37}$$

where $\mathscr{I}_Y(\cdot) = \int_{-h}^h (\cdot) \, \mathrm{d}\tilde{Y}$ indicates integration of a function through the thickness of the ionomer.

Balance equations are obtained from the stationarity of the TPE in Eq. (37). Specifically, BVPs with natural boundary conditions for the unknown functions $u_0^i(X)$, $w_0^i(X)$, and p(X) are found by imposing that the first variation of the TPE with respect to each variable is equal to zero [45]. More in detail, we compute the first variation of the TPE in Eq. (37) with respect to the desired function, set it to zero, integrate by parts the terms that contain the derivative of the variation of the unknown function, and impose that the equality must hold for any choice of its variation.

From the first variation of the TPE with respect to $u_0^{\rm i}(X)$, we obtain the following differential problem:

$$A_{u_0}u_{0,XY}^{i} + B_{u_0}p_{,X} + C_{u_0}p_{,XXX} = 0, (38a)$$

$$A_{u_0}u_{0X}^{i}(0) + B_{u_0}p(0) + C_{u_0}p_{XX}(0) + \mathcal{I}_Y(\sigma_{0XY}) = 0$$
 or $u_0^{i}(0)$ imposed, (38b)

$$A_{u_0}u_{0,Y}^{i}(l) + B_{u_0}p(l) + C_{u_0}p_{XX}(l) + \mathcal{I}_{Y}(\sigma_{0,Y}) = 0$$
 or $u_0^{i}(l)$ imposed, (38c)

where coefficients are listed in the column " u_0 " in Tab. 2.

By setting to zero the first variation of the TPE with respect to $w_0^i(X)$, we find

$$A_{w_0} w_{0,XXXX}^{i} + B_{w_0} p_{XXXX} + C_{w_0} p_{XX} = 0, (39a)$$

$$A_{w_0} w_{0,YYY}^i(0) + B_{w_0} p_{XXX}(0) + C_{w_0} p_{X}(0) = 0$$
 or $w_0^i(0)$ imposed, (39b)

$$A_{w_0} w_{0,YYY}^i(l) + B_{w_0} p_{XXX}(l) + C_{w_0} p_{X}(l) = 0$$
 or $w_0^i(l)$ imposed, (39c)

$$A_{w_0}w_{0,XX}^i(0) + B_{w_0}p_{XX}(0) + C_{w_0}p(0) - \mathscr{I}_Y(\sigma_{0_{XX}}Y) = 0$$
 or $w_{0,X}^i(0)$ imposed, (39d)

$$A_{w_0} w_{0,XX}^i(l) + B_{w_0} p_{XX}(l) + C_{w_0} p(l) - \mathscr{I}_Y(\sigma_{0_{XX}} Y) = 0$$
 or $w_{0,X}^i(l)$ imposed. (39e)

The coefficients of this BVP are tabulated in Tab. 2, in the column " w_0 ".

Finally, by examining the variation of the TPE with respect to p(X), we establish

$$A_{p}p_{,XXXX} + B_{p}p_{,XX} + C_{p}p + D_{p}w_{0,XXXX}^{i} + E_{p}w_{0,XX}^{i} + F_{p}u_{0,XXX}^{i} + G_{p}u_{0,X}^{i} + \mathscr{I}_{Y}(\sigma_{0_{YY}}\bar{f}_{,Y}) = 0,$$
(40a)

$$A_p p_{,XXX}(0) + B_p p_{,X}(0) + D_p w_{0,XXX}^i(0) + F_p u_{0,XX}^i(0) = 0$$
 or $p(0)$ imposed, (40b)

$$A_p p_{XXX}(l) + B_p p_X(l) + D_p w_{0,XXX}^i(l) + F_p u_{0,XX}^i(l) = 0$$
 or $p(l)$ imposed, (40c)

$$A_p p_{,XX}(0) + D_p w_{0,XX}^i(0) + F_p u_{0,X}^i(0) = 0$$
 or $p(0)_{,X}$ imposed, (40d)

$$A_p p_{,XX}(l) + D_p w_{0,XX}^i(l) + F_p u_{0,X}^i(l) = 0$$
 or $p(l)_X$ imposed, (40e)

whose coefficients are given in the column "p" in Tab. 2.

Table 2 Coefficients for the displacement of the ionomer in the enriched Euler-Bernoulli model in Eqs. (38), (39), and (40).

Since we consider $\bar{f}(Y)$ as a known function, the BVPs in Eqs. (38), (39), and (40) are all linear. Predictably, the BVP for the longitudinal displacement of the mid-axis, $u_0^i(X)$, does not contain any term with the transverse displacement of the mid-axis, $w_0^i(X)$. Extension and bending are only indirectly coupled through p(X), which modifies the classical second and fourth order differential equations describing extension and bending in Euler-Bernoulli beam theory. The coefficients multiplying the derivatives of $u_0^i(X)$ and $w_0^i(X)$ in Eq. (38) and (39) represent the axial and bending stiffness of the IPMC, respectively. Both of these quantities depend on a combination of the mechanical properties of the ionomer and electrodes.

The BVP for p(X) in Eq. (40) displays much more complex couplings than the other two BVPs, as it contains terms with odd derivatives of the longitudinal displacement of the mid-axis $u_0^i(X)$ and even derivatives of the transverse displacement of the mid-axis $w_0^i(X)$. Interestingly, should we discard the presence of the electrodes (that is, e=0), the order of the BVP for p(X) would reduce from four to two. This observation suggests that the presence of the electrodes qualitatively affects multiaxial deformations in IPMCs, increasing the complexity of the problem. Similarly, the highest derivatives of p(X) in Eqs. (38) and (39), and those of $u_0^i(X)$ and $w_0^i(X)$ in Eq. (40) would disappear, further simplifying the BVPs.

The forcing terms associated with the eigenstress components $\sigma_{0_{XX}}$ and $\sigma_{0_{YY}}$ enter the equations in two different ways. Specifically, $\sigma_{0_{XX}}$ appears only in the boundary conditions of Eqs. (38) and (39), as the resultant axial force and bending moment, respectively. This is a consequence of the fact that $\sigma_{0_{XX}}$ does not depend on the axial coordinate X. On the

other hand, $\sigma_{0_{YY}}$ appears directly in the differential equation in Eq. (40), scaled by $\bar{f}_{,Y}(Y)$ and integrated along the thickness, without appearing in any boundary condition.

Due to the relative simplicity of the linear BVPs in Esq. (38), (39), and (40), it is possible to compute a closed-form solution for specific boundary and loading conditions. This computation is tackled in Section 4.1.1.

3.2.2 Original and enriched enhanced high-order sandwich panel theories

While the original and enriched Euler-Bernoulli beam theories provide a simple, analytically-tractable description of IPMC actuation, their validity may be limited by low-order representation of the ionomer deformation. In fact, IPMCs share similarities with sandwich-like structures used in aerospace applications, formed by a core between two stiffer skins. In these composite structures, shear deformability of the core may play a dramatic role in the response of the sandwich, which is not captured by low-order theories [33, 34, 37]. Modeling the mechanical response of sandwich structures becomes even more challenging if the core is soft, that is, if the transverse deformation is relevant [38, 39, 40, 43].

In order to account for the core deformability, we should rely on higher-order theories, like the original EHOSPT proposed by Phan et al. [43] to retrieve shear deformations in sandwich structures. Within this framework, the displacement field of the ionomer is described by seven functions of the axial coordinate X, four for the longitudinal displacement and three for the transverse displacement, namely,

$$u^{i}(X,Y) = u_{0}^{i}(X) + u_{1}^{i}(X)Y + u_{2}^{i}(X)Y^{2} + u_{3}^{i}(X)Y^{3},$$
(41a)

$$w^{i}(X,Y) = w_{0}^{i}(X) + w_{1}^{i}(X)Y + w_{2}^{i}(X)Y^{2}.$$
 (41b)

By retaining the second order power in the expansion for the transverse displacement in Eq. (41b), the original EHOSPT accounts for through-the-thickness contraction with an affine dependence on Y. The possibility of describing parabolic thickness contraction is important for separately tracking the motion of the two skins that could be triggered under severe boundary conditions [39], for example, when loading only one of the skins of the sandwich. When compared with the original Euler-Bernoulli beam theory, this theory encapsulates shear deformations and warping of the cross-section, which is allowed to rotate about the mid-axis $(u_1^i(X) \neq -w_0^i(X)_X)$ and parabolically deform. When examining the longitudinal displacement in Eq. (41b), the theory enables a much more complex behavior than original Euler-Bernoulli beam theory, including a cubic dependence on the through-the-thickness coordinate Y on top of the mid-axis translation and cross-section rigid rotation.

With respect to strain fields, the original EHOSPT enables cubic variations of the axial strain along the ionomer thickness, compared to the linear profiles of the original Euler-Bernoulli beam theory. The through-the-thickness strain, completely absent from the original Euler-Bernoulli, has a linear through-the-thickness profile in the original EHOSPT. Shear strains consist of a second-order polynomial in Y, whose coefficients are function of X that combine terms from longitudinal and transverse displacements in Eq. (41).

Similar to the previous Subsection, we consider an enriched version of the EHOSPT where we add the localized through-the-thickness strain near the electrodes, modulated by an unknown function of the axial coordinate, p(X). In the following, we only derive the governing equations for the enriched EHOSPT, that is,

$$u^{i}(X,Y) = u_{0}^{i}(X) + u_{1}^{i}(X)Y + u_{2}^{i}(X)Y^{2} + u_{3}^{i}(X)Y^{3}, \tag{42a}$$

$$w^{i}(X,Y) = w_{0}^{i}(X) + w_{1}^{i}(X)Y + w_{2}^{i}(X)Y^{2} + p(X)\bar{f}(Y), \tag{42b}$$

which are associated with the following strains, computed from Eq. (18):

$$\varepsilon_{XX}^{i}(X,Y) = u_{0,X}^{i}(X) + u_{1,X}^{i}(X)Y + u_{2,X}^{i}(X)Y^{2} + u_{3,X}^{i}(X)Y^{3}, \tag{43a}$$

$$\varepsilon_{YY}^{i}(X,Y) = w_1^{i}(X) + 2w_2^{i}(X)Y + p(X)\bar{f}_{,Y}(Y),$$
 (43b)

$$\begin{aligned} \gamma_{XY}^{i}(X,Y) &= [u_{1}^{i}(X) + w_{0}^{i}(X)_{,X}] + [2u_{2}^{i}(X) + w_{1}^{i}(X)_{,X}]Y \\ &+ [3u_{3}^{i}(X) + w_{2}^{i}(X)_{,X}]Y^{2} + p_{,X}(X)\bar{f}(Y). \end{aligned} \tag{43c}$$

Original EHOSPT without localized through-the-thickness strain in Eq. (41) can be computed by setting $\bar{f}(Y) = 0$.

By considering the Euler-Bernoulli beam model for the electrodes in Eq. (28), imposing the matching conditions in Eq. (25), and utilizing Eq. (42), we express the displacement field of the electrodes as a function of that of the core, whereby

$$u^{\text{el}^+}(X,Y) = u_0^{\text{i}}(X) + u_1^{\text{i}}(X)h + u_2^{\text{i}}(X)h^2 + u_3^{\text{i}}(X)h^3 - (Y - h)[w_0^{\text{i}}_X(X) + w_{1,X}^{\text{i}}(X)h + w_{2,X}^{\text{i}}(X)h^2 + p_X(X)\bar{f}(h)],$$
(44a)

$$u^{\mathrm{el}^{-}}(X,Y) = u_{0}^{\mathrm{i}}(X) - u_{1}^{\mathrm{i}}(X)h + u_{2}^{\mathrm{i}}(X)h^{2} - u_{3}^{\mathrm{i}}(X)h^{3} - (Y+h)[w_{0}^{\mathrm{i}}(X) - w_{1}^{\mathrm{i}}(X)h + w_{2}^{\mathrm{i}}(X)h^{2} + p_{X}(X)\bar{f}(-h)],$$

$$(44b)$$

$$w^{\text{el}^+}(X,Y) = w_0^{\text{i}}(X) + w_1^{\text{i}}(X)h + w_2^{\text{i}}(X)h^2 + p(X)\bar{f}(h), \tag{44c}$$

$$w^{el^{-}}(X,Y) = w_0^{i}(X) - w_1^{i}(X)h + w_2^{i}(X)h^2 + p(X)\bar{f}(-h). \tag{44d}$$

The axial strain of the electrodes, from Eq. (18), is given by

$$\varepsilon_{XX}^{\text{el}^{\pm}} = u_{0,X}^{\text{i}}(X) \pm u_{1,X}^{\text{i}}(X)h + u_{2,X}^{\text{i}}(X)h^{2} \pm u_{3,X}^{\text{i}}(X)h^{3} - (Y \pm h)[w_{0,XX}^{\text{i}}(X) \pm w_{1,XX}^{\text{i}}(X)h + w_{2,XX}^{\text{i}}(X)h^{2} + p_{,XX}(X)\bar{f}(\pm h)].$$
(45)

From Eq. (44), we note that the electrodes follow the longitudinal and transverse displacements of the ionomer-electrode interfaces, with an additional term describing the rotation of their cross-sections, caused by the transverse displacement of the interfaces varying along the IPMC axis.

By substituting Eqs. (43) and (45) into Eqs. (27), (29), and (31), we obtain the TPE,

$$\begin{split} U &= \frac{1}{2} \int_{S^{i}} \left\{ (\lambda_{L} + 2\mu_{L}) \left[(u_{0,X}^{i} + u_{1,X}^{i}Y + u_{2,X}^{i}Y^{2} + u_{3,X}^{i}Y^{3})^{2} + (w_{1}^{i} + 2Yw_{2}^{i} + p\bar{f}_{,Y})^{2} \right] \right. \\ &+ 2\lambda_{L} (u_{0,X}^{i} + u_{1,X}^{i}Y + u_{2,X}^{i}Y^{2} + u_{3,X}^{i}Y^{3}) (w_{1}^{i} + 2Yw_{2}^{i} + p\bar{f}_{,Y}) \\ &+ \mu_{L} (u_{1}^{i} + 2Yu_{2}^{i} + 3Y^{2}u_{3}^{i} + p_{,X}\bar{f} + w_{0,X}^{i} + w_{1,X}^{i}Y + w_{2,X}^{i}Y^{2})^{2} \right\} dS^{i} \\ &+ \frac{1}{2} \int_{\mathscr{S}^{el^{+}}} Y_{el}^{\prime} \left[u_{0,X}^{i} + u_{1,X}^{i}h + u_{2,X}^{i}h^{2} + u_{3,X}^{i}h^{3} \right. \\ &- (Y - h) \left[w_{0,XX}^{i} + w_{1,XX}^{i}h + w_{2,XX}^{i}h^{2} + p_{,XX}\bar{f}(h) \right] \right]^{2} dS^{+} \\ &+ \frac{1}{2} \int_{\mathscr{S}^{el^{-}}} Y_{el}^{\prime} \left[u_{0,X}^{i} - u_{1,X}^{i}h + u_{2,X}^{i}h^{2} - u_{3,X}^{i}h^{3} \right. \\ &- (Y + h) \left[w_{0,XX}^{i} - w_{1,XX}^{i}h + w_{2,XX}^{i}h^{2} + p_{,XX}\bar{f}(-h) \right] \right]^{2} dS^{-} \\ &+ \int_{S^{i}} \left[\sigma_{0XX} (u_{0,X}^{i} + u_{1,X}^{i}Y + u_{2,X}^{i}Y^{2} + u_{3,X}^{i}Y^{3}) + \sigma_{0YY} (w_{1}^{i} + 2Yw_{2}^{i} + p\bar{f}_{,Y}) \right] dS^{i}. \end{split}$$

The governing equations for each of the seven functions describing the displacement field of the core, together with the axial variation of the through-the-thickness contraction, are obtained by imposing the stationarity of the TPE in Eq. (46), following the same procedure of Section 3.2.1. Below, we list the equations associated with the first variation of the TPE with respect to each variable, whose coefficients are collected in Tabs. 3 and 4.

 $- u_0^{i}$:

$$A'_{u_0}u^{i}_{0,XX} + B'_{u_0}u^{i}_{2,XX} + C'_{u_0}w^{i}_{1,X} + D'_{u_0}w^{i}_{1,XXX} + E'_{u_0}p_{,XXX} + F'_{u_0}p_{,X} = 0,$$
 (47a)

$$A'_{u_0}u^{i}_{0,X}(0) + B'_{u_0}u^{i}_{2,X}(0) + C'_{u_0}w^{i}_{1}(0) + D'_{u_0}w^{i}_{1,XX}(0) + E'_{u_0}p_{,XX}(0) + F'_{u_0}p(0) + \mathscr{I}_{Y}(\sigma_{0_{YY}}) = 0 \qquad \text{or } u^{i}_{0}(0) \text{ imposed,}$$

$$(47b)$$

$$A'_{u_0}u_{0,X}^{i}(l) + B'_{u_0}u_{2,X}^{i}(l) + C'_{u_0}w_{1}^{i}(l) + D'_{u_0}w_{1,XX}^{i}(l) + E'_{u_0}p_{,XX}(l) + F'_{u_0}p(l) + \mathscr{I}_{Y}(\sigma_{0_{XY}}) = 0 \quad \text{or } u_{0}^{i}(l) \text{ imposed;}$$

$$(47c)$$

 $- u_1^{i}$:

$$A'_{u_{1}}u_{1,XX}^{i} + B'_{u_{1}}u_{3,XX}^{i} + (C'_{u_{1}} + D'_{u_{1}})w_{2,X}^{i} + (E'_{u_{1}} + F'_{u_{1}})p_{,X} + G'_{u_{1}}w_{0,X}^{i} + G'_{u_{1}}u_{1}^{i} + H'_{u_{1}}u_{3}^{i} + I'_{u_{1}}w_{0,XXX}^{i} + J'_{u_{1}}w_{2,XXX}^{i} + K'_{u_{1}}p_{,XXX} = 0,$$

$$(48a)$$

$$A'_{u_{1}}u_{1,X}^{i}(0) + B'_{u_{1}}u_{3,X}^{i}(0) + C'_{u_{1}}w_{2}^{i}(0) + E'_{u_{1}}p(0) + I'_{u_{1}}w_{0,XX}^{i}(0) + J'_{u_{1}}w_{2,XX}^{i}(0) + K'_{u_{1}}p_{XX}(0) + \mathscr{I}_{Y}(\sigma_{0_{XY}}Y) = 0 \qquad \text{or } u_{1}^{i}(0) \text{ imposed,}$$

$$(48b)$$

$$\begin{split} A'_{u_1}u^{\mathbf{i}}_{1,X}(l) + B'_{u_1}u^{\mathbf{i}}_{3,X}(l) + C'_{u_1}w^{\mathbf{i}}_{2}(l) + E'_{u_1}p(l) + I'_{u_1}w^{\mathbf{i}}_{0,XX}(l) + J'_{u_1}w^{\mathbf{i}}_{2,XX}(l) \\ + K'_{u_1}p_{,XX}(l) + \mathscr{I}_{Y}(\sigma_{0_{XX}}Y) &= 0 \qquad \text{or } u^{\mathbf{i}}_{1}(l) \text{ imposed;} \end{split} \tag{48c}$$

- *u*ⁱ₂:

$$A'_{u_{2}}u^{i}_{0,XX} + B'_{u_{2}}u^{i}_{2,XX} + (C'_{u_{2}} + D'_{u_{2}})w^{i}_{1,X} + (E'_{u_{2}} + F'_{u_{2}})p_{,X} + G'_{u_{2}}u^{i}_{2} + H'_{u_{2}}w^{i}_{1,XXX} + I'_{u_{2}}p_{,XXX} = 0,$$
(49a)

$$\begin{split} A'_{u_2}u^{\mathrm{i}}_{0,X}(0) + B'_{u_2}u^{\mathrm{i}}_{2,X}(0) + C'_{u_2}w^{\mathrm{i}}_{1}(0) + E'_{u_2}p(0) + H'_{u_2}w^{\mathrm{i}}_{1,XX}(0) \\ + I'_{u_2}p_{,XX}(0) + \mathscr{I}_{Y}(\sigma_{0_{XX}}Y^2) &= 0 \qquad \text{or } u^{\mathrm{i}}_{2}(0) \text{ imposed}, \end{split} \tag{49b}$$

$$A'_{u_{2}}u_{0,X}^{i}(l) + B'_{u_{2}}u_{2,X}^{i}(l) + C'_{u_{2}}w_{1}^{i}(l) + E'_{u_{2}}p(l) + H'_{u_{2}}w_{1,XX}^{i}(l) + I'_{u_{2}}p_{,XX}(l) + \mathscr{I}_{Y}(\sigma_{0_{YY}}Y^{2}) = 0 \quad \text{or } u_{2}^{i}(l) \text{ imposed;}$$

$$(49c)$$

 $- u_3^{i}$:

$$A'_{u_{3}}u_{1,XX}^{i} + B'_{u_{3}}u_{3,XX}^{i} + (C'_{u_{3}} + D'_{u_{3}})w_{2,X}^{i} + (E'_{u_{3}} + F'_{u_{3}})p_{,X} + G'_{u_{3}}u_{1}^{i} + G'_{u_{3}}w_{0,X}^{i} + H'_{u_{3}}u_{3}^{i} + I'_{u_{3}}w_{0,XXX}^{i} + J'_{u_{3}}w_{2,XXX}^{i} + K'_{u_{3}}p_{,XXX} = 0,$$
 (50a)

$$A'_{u_{3}}u_{1,X}^{i}(0) + B'_{u_{3}}u_{3,X}^{i}(0) + C'_{u_{3}}w_{2}^{i}(0) + E'_{u_{3}}p(0) + I'_{u_{3}}w_{0,XX}^{i}(0) + J'_{u_{3}}w_{2,XX}^{i}(0) + K'_{u_{2}}p_{XX}(0) + \mathscr{I}_{Y}(\sigma_{0_{XX}}Y^{3}) = 0 \quad \text{or } u_{3}^{i}(0) \text{ imposed,}$$

$$(50b)$$

$$\begin{split} A'_{u_3}u^{\rm i}_{1,X}(l) + B'_{u_3}u^{\rm i}_{3,X}(l) + C'_{u_3}w^{\rm i}_{2}(l) + E'_{u_3}p(l) + I'_{u_3}w^{\rm i}_{0,XX}(l) + J'_{u_3}w^{\rm i}_{2,XX}(l) \\ + K'_{u_3}p_{,XX}(l) + \mathscr{I}_Y(\sigma_{0_{XX}}Y^3) &= 0 \qquad \text{or } u^{\rm i}_{3}(l) \text{ imposed;} \end{split} \tag{50c}$$

 $- w_0^{i}$:

$$A'_{w_0}w_{0,XXXX}^{i} + B'_{w_0}w_{2,XXXX}^{i} + C'_{w_0}u_{1,XXX}^{i} + D'_{w_0}u_{3,XXX}^{i} + E'_{w_0}u_{1,X}^{i} + E'_{w_0}w_{0,XX}^{i} + F'_{w_0}u_{3,X}^{i} + G'_{w_0}p_{,XX} + H'_{w_0}w_{2,XX}^{i} + I'_{w_0}p_{,XXXX} = 0,$$
(51a)

$$\begin{split} A'_{w_0}w^{\mathrm{i}}_{0,XXX}(0) + B'_{w_0}w^{\mathrm{i}}_{2,XXX}(0) + C'_{w_0}u^{\mathrm{i}}_{1,XX}(0) + D'_{w_0}u^{\mathrm{i}}_{3,XX}(0) \\ + E'_{w_0}u^{\mathrm{i}}_{1}(0) + E'_{w_0}w^{\mathrm{i}}_{0,X}(0) + F'_{w_0}u^{\mathrm{i}}_{3}(0) + G'_{w_0}p_{,x}(0) \\ + H'_{w_0}w^{\mathrm{i}}_{2,X}(0) + I'_{w_0}p_{,XXX}(0) = 0 \qquad \text{or } w^{\mathrm{i}}_{0}(0) \text{ imposed}, \end{split} \tag{51b}$$

$$\begin{split} A'_{w_0}w^{\mathbf{i}}_{0,XXX}(l) + B'_{w_0}w^{\mathbf{i}}_{2,XXX}(l) + C'_{w_0}u^{\mathbf{i}}_{1,XX}(l) + D'_{w_0}u^{\mathbf{i}}_{3,XX}(l) \\ + E'_{w_0}u^{\mathbf{i}}_{1}(l) + E'_{w_0}w^{\mathbf{i}}_{0,X}(l) + F'_{w_0}u^{\mathbf{i}}_{3}(l) + G'_{w_0}p_{,X}(l) \\ + H'_{w_0}w^{\mathbf{i}}_{2,X}(l) + I'_{w_0}p_{,XXX}(l) = 0 \qquad \text{or } w^{\mathbf{i}}_{0}(l) \text{ imposed}, \end{split} \tag{51c}$$

$$A'_{w_0}w^{\mathbf{i}}_{0,XX}(0) + B'_{w_0}w^{\mathbf{i}}_{2,XX}(0) + C'_{w_0}u^{\mathbf{i}}_{1,X}(0) + D'_{w_0}u^{\mathbf{i}}_{3,X}(0) + I'_{w_0}p_{,XX}(0) = 0 \qquad \text{or } w^{\mathbf{i}}_{0,X}(0) \text{ imposed,}$$

$$(51d)$$

$$\begin{split} A'_{w_0} w^{\mathbf{i}}_{0,XX}(l) + B'_{w_0} w^{\mathbf{i}}_{2,XX}(l) + C'_{w_0} u^{\mathbf{i}}_{1,X}(l) + D'_{w_0} u^{\mathbf{i}}_{3,X}(l) \\ + I'_{w_0} p_{,XX}(l) = 0 \qquad \text{or } w^{\mathbf{i}}_{0,X}(l) \text{ imposed;} \end{split} \tag{51e}$$

 $- w_1^i$:

$$\begin{split} A'_{w_{1}}w_{1,XXXX}^{i} + B'_{w_{1}}u_{0,XXX}^{i} + C'_{w_{1}}u_{2,XXX}^{i} + D'_{w_{1}}w_{1}^{i} + E'_{w_{1}}p + F'_{w_{1}}u_{0,X}^{i} + (G'_{w_{1}} + H'_{w_{1}})u_{2,X}^{i} \\ + I'_{w_{1}}p_{,XX} + J'_{w_{1}}w_{1,XX}^{i} + K'_{w_{1}}p_{,XXXX} + \mathscr{I}_{Y}(\sigma_{0_{YY}}) &= 0, \end{split}$$
 (52a)

$$A'_{w_1}w_{1,XXX}^{i}(0) + B'_{w_1}u_{0,XX}^{i}(0) + C'_{w_1}u_{2,XX}^{i}(0) + H'_{w_1}u_{2}^{i}(0) + I'_{w_1}p_{,X}(0) + J'_{w_1}w_{1,X}^{i}(0) + K'_{w_1}p_{,XXX}(0) = 0 or w_{1}^{i}(0) imposed,$$
 (52b)

$$\begin{split} A'_{w_{1}}w_{1,XXX}^{i}(l) + B'_{w_{1}}u_{0,XX}^{i}(l) + C'_{w_{1}}u_{2,XX}^{i}(l) + H'_{w_{1}}u_{2}^{i}(l) + I'_{w_{1}}p_{,X}(l) \\ + J'_{w_{1}}w_{1,X}^{i}(l) + K'_{w_{1}}p_{,XXX}(l) = 0 \qquad \text{or } w_{1}^{i}(l) \text{ imposed,} \end{split}$$
 (52c)

$$A'_{w_1}w^{i}_{1,XX}(0) + B'_{w_1}u^{i}_{0,X}(0) + C'_{w_1}u^{i}_{2,X}(0) + K'_{w_1}p_{,XX}(0) = 0$$
 or $w^{i}_{1,X}(0)$ imposed,

$$A'_{w_1}w_{1,XX}^{i}(l) + B'_{w_1}u_{0,X}^{i}(l) + C'_{w_1}u_{2,X}^{i}(l) + K'_{w_1}p_{,XX}(l) = 0 or w_{1,X}^{i}(l) imposed; (52e)$$

 $- w_{2}^{i}$:

$$\begin{split} A'_{w_{2}}w^{\mathrm{i}}_{0,XXXX} + B'_{w_{2}}w^{\mathrm{i}}_{2,XXXX} + C'_{w_{2}}u^{\mathrm{i}}_{1,XXX} + D'_{w_{2}}u^{\mathrm{i}}_{3,XXX} + E'_{w_{2}}w^{\mathrm{i}}_{2} + F'_{w_{2}}p \\ & + (G'_{w_{2}} + H'_{w_{2}})u^{\mathrm{i}}_{1,X} + H'_{w_{2}}w^{\mathrm{i}}_{0,XX} + (I'_{w_{2}} + J'_{w_{2}})u^{\mathrm{i}}_{3,X} + K'_{w_{2}}p_{,XX} \\ & + L'_{w_{2}}w^{\mathrm{i}}_{2,XX} + M'_{w_{2}}p_{,XXXX} + 2\mathscr{I}_{Y}(\sigma_{0_{YY}}Y) = 0, \end{split} \tag{53a}$$

$$\begin{split} A'_{w_2}w^{\mathrm{i}}_{0,XXX}(0) + B'_{w_2}w^{\mathrm{i}}_{2,XXX}(0) + C'_{w_2}u^{\mathrm{i}}_{1,XX}(0) + D'_{w_2}u^{\mathrm{i}}_{3,XX}(0) \\ + H'_{w_2}u^{\mathrm{i}}_{1}(0) + H'_{w_2}w^{\mathrm{i}}_{0,X}(0) + J'_{w_2}u^{\mathrm{i}}_{3}(0) + K'_{w_2}p_{,X}(0) \\ + L'_{w_2}w^{\mathrm{i}}_{2,X}(0) + M'_{w_2}p_{,XXX}(0) = 0 \qquad \text{or } w^{\mathrm{i}}_{2}(0) \text{ imposed,} \end{split}$$
 (53b)

$$\begin{split} A'_{w_{2}}w_{0,XXX}^{i}(l) + B'_{w_{2}}w_{2,XXX}^{i}(l) + C'_{w_{2}}u_{1,XX}^{i}(l) + D'_{w_{2}}u_{3,XX}^{i}(l) \\ + H'_{w_{2}}u_{1}^{i}(l) + H'_{w_{2}}w_{0,X}^{i}(l) + J'_{w_{2}}u_{3}^{i}(l) + K'_{w_{2}}p_{,X}(l) \\ + L'_{w_{2}}w_{2,X}^{i}(l) + M'_{w_{2}}p_{,XXX}(l) = 0 \qquad \text{or } w_{2}^{i}(l) \text{ imposed,} \end{split}$$
 (53c)

$$A'_{w_{2}}w_{0,XX}^{i}(0) + B'_{w_{2}}w_{2,XX}^{i}(0) + C'_{w_{2}}u_{1,X}^{i}(0) + D'_{w_{2}}u_{3,X}^{i}(0) + M'_{w_{2}}p_{,XX}(0) = 0 mtext{or } w_{2,X}^{i}(0) mtext{ imposed,}$$
 (53d)

- p:

$$A'_{p}p_{,XXXX} + B'_{p}p_{,XX} + C'_{p}p + D'_{p}u^{i}_{0,XXX} + E'_{p}u^{i}_{1,XXX} + F'_{p}u^{i}_{2,XXX} + G'_{p}u^{i}_{3,XXX} + H'_{p}w^{i}_{0,XXXX} + I'_{p}w^{i}_{1,XXXX} + J'_{p}w^{i}_{2,XXXX} + K'_{p}w^{i}_{1} + L'_{p}w^{i}_{2} + M'_{p}u^{i}_{0,X} + (N'_{p} + O'_{p})u^{i}_{1,X} + O'_{p}w^{i}_{0,XX} + (P'_{p} + Q'_{p})u^{i}_{2,X} + (R'_{p} + S'_{p})u^{i}_{3,X} + T'_{p}w^{i}_{1,XX} + U'_{p}w^{i}_{2,XX} + \mathscr{I}_{Y}(\sigma_{0yy}\bar{f}_{,Y}) = 0,$$
 (54a)

$$\begin{split} A'_p p_{,XXX}(0) + B'_p p_{,X}(0) + D'_p u^{\mathbf{i}}_{0,XX}(0) + E'_p u^{\mathbf{i}}_{1,XX}(0) + F'_p u^{\mathbf{i}}_{2,XX}(0) + G'_p u^{\mathbf{i}}_{3,XX}(0) \\ + H'_p w^{\mathbf{i}}_{0,XXX}(0) + I'_p w^{\mathbf{i}}_{1,XXX}(0) + J'_p w^{\mathbf{i}}_{2,XXX}(0) + O'_p u^{\mathbf{i}}_{1}(0) + O'_p w^{\mathbf{i}}_{0,X}(0) \\ + Q'_p u^{\mathbf{i}}_{2}(0) + S'_p u^{\mathbf{i}}_{3}(0) + T'_p w^{\mathbf{i}}_{1,X}(0) + U'_p w^{\mathbf{i}}_{2,X}(0) = 0 \qquad \text{or } p(0) \text{ imposed,} \end{split}$$

$$\begin{split} A'_{p}p_{,XXX}(l) + B'_{p}p_{,X}(l) + D'_{p}u^{\mathrm{i}}_{0,XX}(l) + E'_{p}u^{\mathrm{i}}_{1,XX}(l) + F'_{p}u^{\mathrm{i}}_{2,XX}(l) + G'_{p}u^{\mathrm{i}}_{3,XX}(l) \\ + H'_{p}w^{\mathrm{i}}_{0,XXX}(l) + I'_{p}w^{\mathrm{i}}_{1,XXX}(l) + J'_{p}w^{\mathrm{i}}_{2,XXX}(l) + O'_{p}u^{\mathrm{i}}_{1}(l) + O'_{p}w^{\mathrm{i}}_{0,X}(l) \\ + Q'_{p}u^{\mathrm{i}}_{2}(l) + S'_{p}u^{\mathrm{i}}_{3}(l) + T'_{p}w^{\mathrm{i}}_{1,X}(l) + U'_{p}w^{\mathrm{i}}_{2,X}(l) = 0 \qquad \text{or } p(l) \text{ imposed}, \end{split}$$

$$A'_{p}p_{,XX}(0) + D'_{p}u^{i}_{0,X}(0) + E'_{p}u^{i}_{1,X}(0) + F'_{p}u^{i}_{2,X}(0) + G'_{p}u^{i}_{3,X}(0) + H'_{p}w^{i}_{0,XX}(0) + I'_{p}w^{i}_{1,XX}(0) + J'_{p}w^{i}_{2,XX}(0) = 0 \qquad \text{or } p_{,X}(0) \text{ imposed,}$$

$$(54d)$$

$$\begin{split} A'_{p}p_{,XX}(l) + D'_{p}u^{\mathbf{i}}_{0,X}(l) + E'_{p}u^{\mathbf{i}}_{1,X}(l) + F'_{p}u^{\mathbf{i}}_{2,X}(l) + G'_{p}u^{\mathbf{i}}_{3,X}(l) + H'_{p}w^{\mathbf{i}}_{0,XX}(l) \\ + I'_{p}w^{\mathbf{i}}_{1,XX}(l) + J'_{p}w^{\mathbf{i}}_{2,XX}(l) &= 0 \qquad \text{or } p_{,X}(l) \text{ imposed.} \end{split} \tag{54e}$$

Compared to BVPs in Eqs. (38), (39), and (40) for the enriched Euler-Bernoulli model, this system of linear BVPs shows a much more complex structure, with a large number of couplings. Even without considering p(X), the extension of the IPMC, described by the BVP in Eq. (47), is coupled with the higher-order terms in the longitudinal displacement and the linear term in the transverse displacement. A similar claim can be made for IPMC bending in Eq. (48), where the cross-section rotation is coupled to the cubic term in the longitudinal displacement and the even terms in the transverse displacement of the core. The BVP for the mid-axis transverse displacement w_0^i in Eq. (51) shows couplings with the same terms as the cross-section rotation u_1^i , with derivatives of higher orders. For the higher-order terms in the expressions of the longitudinal and transverse displacements in Eq. (42), the BVPs in Eqs. (49), (50), (52), and (53) present even more complex couplings, challenging a physical interpretation of the terms in the equations. In general, we observe

	$ \begin{array}{c} \mu_2 \\ \frac{1}{3} h^2 [(\lambda_L + 2\mu_L) h + 3Y_e'] \\ \frac{3}{5} h^4 [(\lambda_L + 2\mu_L) h + 5Y_e'] e] \\ \frac{3}{5} \lambda_L h^3 \\ -\frac{3}{4} \mu_L h^3 \\ \lambda_L \mathcal{G}_Y (\tilde{f}_Y Y^2) \\ -2\mu_L \mathcal{G}_Y (\tilde{f}_Y Y^2) \\ -\frac{8}{5} \mu_L h^3 \\ -Y_e h^2 e^2 \\ -\frac{1}{2} Y_e h^2 e^2 \\ -\frac{1}{2} Y_e h^2 e^2 \\ \end{array} $	$\begin{array}{c} u_3 \\ \frac{1}{2} h^4 [(\lambda_L + 2\mu_L) h + 5Y_e' e] \\ \frac{1}{2} h^6 [(\lambda_L + 2\mu_L) h + 7Y_e' e] \\ \frac{1}{2} h^4 h^5 \\ -\frac{9}{2} \mu_L h^5 \\ \lambda_L \mathcal{N}_f (\tilde{f}_1 Y Y^3) \\ -3\mu_L \mathcal{N}_f (\tilde{f}_1 Y Y^3) \\ -2\mu_L h^3 \\ -\frac{18}{2} \mu_L h^5 \\ -1$
$-\frac{1}{2}I_{\rm el}^{\prime}ne^{-\left[f(n)+f(-n)\right]}$	1	$-\frac{2}{2}I_{el}n^{2}e^{-}[f(n)+f(-n)]$

Table 3 Coefficients for the longitudinal displacement of the ionomer in the enriched EHOSPT model in Eqs. (47), (48), (49), and (50).

Ь	$Y'_{\rm el} = \frac{e^3}{3} [(\bar{f}(h))^2 + (\bar{f}(-h))^2]$	$-\mu_{ m L} \mathscr{I}_Y(ar{f}^2)$	$(\mathcal{A}_{\!\scriptscriptstyle \mathbf{L}} + 2\mu_{\!\scriptscriptstyle \mathbf{L}})\mathscr{I}_{\!\scriptscriptstyle Y}((ar{f}_{\!\scriptscriptstyle Y})^2)$	$-rac{1}{2}Y_{ m el}^{\prime}e^{2}\mathscr{I}_{Y}(ar{f}_{Y})$	$-\frac{1}{2}Y'_{\rm el}he^2[\bar{f}(h)+\bar{f}(-h)]$	$-rac{1}{2}Y_{ m el}'h^2e^2\mathscr{I}_Y(ar{f}_Y)$	$-\frac{1}{2}Y'_{\rm el}h^3e^2[\bar{f}(h)+\bar{f}(-h)]$	$Y_{\rm el}' rac{e^3}{3} \left[ar{f}(h) + ar{f}(-h) ight]$	$Y'_{ m el}hrac{e^3}{3}\mathscr{I}_Y(ar f_Y)$	$Y'_{\rm el}h^2 \frac{e^3}{3} [\bar{f}(h) + \bar{f}(-h)]$	$(\lambda_{\!\scriptscriptstyle L} + 2\mu_{\!\scriptscriptstyle L})\mathscr{I}_{\!\scriptscriptstyle Y}(ar{f}_{\!\scriptscriptstyle Y})$	$2(\lambda_{ m L} + 2\mu_{ m L}) \mathscr{I}_Y(ar{f}_YY)$	$\lambda_{ m L} \mathscr{I}_Y (ar{f}_Y)$	$\lambda_{\rm L}\mathscr{I}_Y(\bar{f}_{,Y}Y)$	$-\mu_{\rm L}\mathscr{I}_Y(\bar{f})$	$\lambda_{\!\scriptscriptstyle L}\mathscr{I}_Y(ar f,_YY^2)$	$-2\mu_{ m L}\mathscr{I}_Y(ar{f}Y)$	$\lambda_{\!L}\mathscr{I}_{\!Y}(ar{f}_{\!Y}Y^3)$	$-3\mu_{ m L}\mathscr{I}_Y(ar{f}Y^2)$	$-\mu_{ m L}\mathscr{I}_Y(ar{f}Y)$	$-\mu_{\rm L}\mathscr{I}_Y(ar{f}Y^2)$
W ₂	$\frac{2}{3}Y_{\rm el}'h^2e^3$	$\frac{2}{3}Y'_{\rm el}h^4e^3$	$-Y'_{\rm el}h^{3}e^{2}$	$-Y'_{ m el}h^5e^2$	$rac{8}{3}(\lambda_{ m L}+2\mu_{ m L})h^3$	$2(\lambda_{ m L} + 2\mu_{ m L}) \mathscr{I}_Y(ar{f}_YY)$	$\frac{4}{3}\lambda_{\rm L}h^3$	$-\frac{2}{3}\mu_{\rm L}h^3$	$\frac{4}{5}\lambda_{\rm L}h^5$	$-\frac{6}{5}\mu_{\rm L}h^5$	$-\mu_{ m L} \mathscr{I}_Y(ar{f}Y^2)$	$-\frac{2}{5}\mu_{\rm L}h^5$	$Y'_{\rm el}h^2 \frac{e^3}{3} [\bar{f}(h) + \bar{f}(-h)]$								
w_1	$\frac{2}{3}Y_{\rm el}'h^2e^3$	$-Y'_{ m el}he^2$	$-Y'_{\rm el}h^3e^2$	$2(\lambda_{ m L} + 2\mu_{ m L})h$	$(\lambda_{\!\scriptscriptstyle L} + 2\mu_{\!\scriptscriptstyle L})\mathscr{I}_Y(ar f_Y)$	$2\lambda_{\rm L}h$	$\frac{2}{3}\lambda_{\rm L}h^3$	$-\frac{4}{3}\mu_{\rm L}h^{3}$	$-\mu_{\rm L}\mathscr{I}_{\rm Y}(\bar{f}Y)$	$-\frac{2}{3}\mu_{\rm L}h^3$	$Y'_{ m el} h rac{e^3}{3} \mathscr{I}_Y(ar{f}_Y)$										
W_0	$\frac{2}{3}Y_{\rm el}'e^3$	$\frac{2}{3}Y'_{\rm el}h^2e^3$	$-Y'_{ m el}he^2$	$-Y'_{\rm el}h^3e^2$	$-2\mu_{ m L}h$	$-2\mu_{\rm L}h^3$	$-\mu_{\rm L}\mathscr{I}_Y(\bar{f})$	$-rac{2}{3}\mu_{ m L}h^3$	$Y'_{\rm el} \frac{e^3}{3} [\bar{f}(h) + \bar{f}(-h)]$												
	$A'_{(\cdot)}$	$B_{(\cdot)}'$	<u>ئ</u>	$D_{(\cdot)}^{(\cdot)}$	$E_{(\cdot)}'$	$F_{(\cdot)}'$		$H_{(\cdot)}^{(\cdot)}$	<i>I</i> (:)	<i>F</i>	$K'_{(\cdot)}$	$L_{(\cdot)}^{(\cdot)}$	$M_{(\cdot)}'$	 "	, (O)	P (:)	<i>Q</i> (:)	R (.)	S (:)	T_{\odot}	

Table 4 Coefficients for the transverse displacement of the ionomer in the enriched EHOSPT model in Eqs. (51), (52), (53), and (54).

that odd (even) terms in the longitudinal displacement only couple to even (odd) terms in the transverse displacement, and vice versa, similar to what observed in the shear strain in Eq. (43c).

The BVP in Eq. (54) for p(X) presents the largest number of couplings. Contrary to all the other BVPs, in this case, all the terms in the longitudinal and transverse displacements appear in the differential equation. Should one utilize the original EHOSPT, odd (even) terms in the longitudinal displacement in Eq. (42a) would not interact with the even (odd) terms in the same expression and with odd (even) terms in the transverse displacement in Eq. (42b), and vice versa.

Similar to enriched Euler-Bernoulli beam theory, the presence of the electrodes further exacerbates the overall scenario. Based on the coefficients in Tabs. 3 and 4, we comment that several terms with high-order derivatives in all the BVPs would disappear with zero-thickness electrodes. In particular, as for enriched Euler-Bernoulli beam theory, neglecting the presence of the electrodes would reduce the fourth-order BVP in Eq. (54) to a second-order problem. This observation suggests that the electrodes modify multiaxial deformations in IPMCs not only quantitatively, by increasing the stiffness associated with IPMC axial deformations (see coefficients $A'_{(\cdot)}$ and $B'_{(\cdot)}$ in Tab. 3), but also qualitatively.

The eigenstress components $\sigma_{0_{XX}}$ and $\sigma_{0_{YY}}$ are present as forcing terms in all BVPs but the one for the mid-axis transverse displacement in Eq. (51). Similar to the treatment of Euler-Bernoulli beam theory, $\sigma_{0_{XX},X}$ does not appear in the differential equations of the BVPs in Eqs. (47), (48), (49), and (50), as it is constant along X. On the other hand, terms in $\sigma_{0_{XX}}$ multiplied by increasing powers of Y and integrated along the thickness are present in the corresponding natural boundary conditions of the same BVPs. We remark that the through-the-thickness eigenstress $\sigma_{0_{YY}}$ never appears in the natural boundary conditions, since $\bar{f}_{,Y}(Y)$ is imposed a-priori. The terms $\sigma_{0_{YY}}$, $\sigma_{0_{YY}}Y$, and $\sigma_{0_{YY}}\bar{f}_{,Y}$, integrated along the thickness of the ionomer, constitute the forcing terms for the differential equations in the BVPs in Eqs. (52), (53), and (54).

The system of coupled linear BVPs for EHOSPT does not allow for a simple closed-form solution, even in the original case. Thereby, we tackle this problem through a Fourier-series approach, similar to that proposed by Pagano [47], in what follows.

4 Solution of structural models and comparison with the fully nonlinear continuum theory

Here, we assess the accuracy of the proposed structural theories through comparison with FE simulations based on the complete nonlinear theory in Cha and Porfiri [29]. We focus on a specific configuration, for which we can obtain a closed-form solution for the enriched Euler-Bernoulli beam theory and a Fourier-series solution for the enriched EHOSPT. In particular, we consider the boundary conditions in Pagano [47], where the end-sections of the IPMC are constrained to move only along the axial direction (Fig. 3). Hence, the ends of the IPMC cannot either rigidly translate transversely nor contract along their thickness. Rigid body motion along the axial direction is blocked by a single-point constraint at the mid-axis. Overall, we impose the following boundary conditions:

$$u^{i}\left(\frac{l}{2},0\right) = 0, (55a)$$

$$w^{i}(0,Y) = 0, Y \in [-h,h],$$
 (55b)

$$w^{i}(l,Y) = 0, Y \in [-h,h],$$
 (55c)

$$w^{\text{el}^{\pm}}(0,Y) = 0, Y \in [-h,h], \tag{55d}$$

$$w^{\text{el}^{\pm}}(l,Y) = 0, Y \in [-h,h].$$
 (55e)

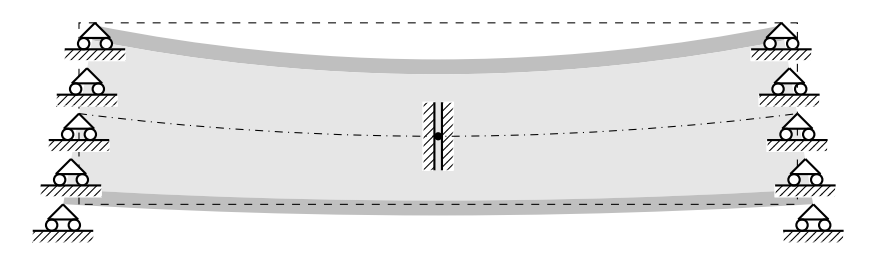


Fig. 3 Schematics of the boundary conditions from Pagano [47], utilized to compute our results. Dashed lines indicate the undeformed configuration, while the dash dotted line represents the IPMC mid-axis.

First, we establish a solution for the enriched Euler-Bernoulli beam theory and for the enriched EHOSPT presented in Sections 3.2.1 and 3.2.2, respectively. Then, we present the results of each structural theory against FE simulations, focusing on both the displacement and stress in the ionomer and electrodes.

4.1 Solution of structural theories

4.1.1 Original and enriched Euler-Bernoulli beam theories

We provide an exact solution for the enriched Euler-Bernoulli model in Section 3.2.1; the solution for the original version can be obtained by setting $\bar{f}(Y) = 0$ in the general solution. The essential boundary conditions in Eq. (55) imply that $w_0^i(0) = 0$, $w_0^i(l) = 0$, p(0) = 0, and p(l) = 0. Accounting for the remaining natural conditions in the systems of BVPs in Eqs. (38), (39), our problem reduces to

$$- u_0^{i}$$
:

$$A_{u_0}u_{0,XX}^{i} + B_{u_0}p_{,X} + C_{u_0}p_{,XXX} = 0, (56a)$$

$$u_0^{\mathbf{i}}\left(\frac{l}{2}\right) = 0,\tag{56b}$$

$$A_{u_0}u_{0X}^{i}(0) + B_{u_0}p(0) + C_{u_0}p_{XX}(0) + \mathcal{I}_Y(\sigma_{0X}) = 0,$$
 (56c)

$$A_{u_0}u_{0,X}^{i}(l) + B_{u_0}p(l) + C_{u_0}p_{XX}(l) + \mathscr{I}_Y(\sigma_{0XX}) = 0,$$
 (56d)

$$- w_0^i$$
:

$$A_{w_0}w_{0,XXXX}^{i} + B_{w_0}p_{,XXXX} + C_{w_0}p_{,XX} = 0, (57a)$$

$$w_0^{\mathbf{i}}(0) = 0, (57b)$$

$$w_0^{\mathbf{i}}(l) = 0,$$
 (57c)

$$A_{w_0} w_{0 XX}^{i}(0) + B_{w_0} p_{XX}(0) + C_{w_0} p(0) - \mathcal{I}_Y(\sigma_{0_{XX}} Y) = 0,$$
 (57d)

$$A_{w_0} w_{0,XX}^{i}(l) + B_{w_0} p_{,XX}(l) + C_{w_0} p(l) - \mathscr{I}_Y(\sigma_{0_{XX}} Y) = 0,$$
 (57e)

- p:

$$A_{p}p_{,XXXX} + B_{p}p_{,XX} + C_{p}p + D_{p}w_{0,XXXX}^{i} + E_{p}w_{0,XX}^{i} + F_{p}u_{0,XXX}^{i} + G_{p}u_{0,X}^{i} + \mathscr{I}_{Y}(\sigma_{0_{YY}}\bar{f}_{,Y}) = 0,$$
(58a)

$$p(0) = 0, (58b)$$

$$p(l) = 0, (58c)$$

$$A_p p_{,XX}(0) + D_p w_{0,XX}^{i}(0) + F_p u_{0,X}^{i}(0) = 0,$$
(58d)

$$A_{p}p_{XX}(l) + D_{p}w_{0YY}^{i}(l) + F_{p}u_{0Y}^{i}(l) = 0.$$
 (58e)

We note that Eq. (56b) does not correspond to any of the essential boundary conditions in Eq. (38), as the IPMC is constrained at the mid-span section rather than at its ends. However, this choice does not affect the solution, as this constraint only blocks the rigid body motion along the axial direction. The overdetermination of the BVP in Eq. (56) is only apparent, whereby imposing the natural boundary condition in Eq. (56c) automatically satisfies Eq. (56d), and vice versa.

As observed in Section 3.2.2, Eqs. (56) and (57) are not directly coupled, such that they can be solved to express $u_0^i(X)$ and $w_0^i(X)$ as a function of p(X). In this way, we can substitute their expressions in Eq. (58) to obtain a BVP in p(X) only. From integration of Eq. (56) with either of the natural boundary conditions in Eqs. (56c) or (56d), we find

$$u_{0,X}^{i}(X) = -\frac{1}{A_{u_0}} \left[\mathscr{I}_Y(\sigma_{0_{XX}}) + B_{u_0} p(X) + C_{u_0} p_{XX}(X) \right]. \tag{59}$$

We note that this expression satisfies both the natural boundary conditions at x = 0 and x = l in the BVP in Eq. (56). On the other hand, by integrating twice Eq. (57) and using the boundary conditions in Eqs. (39d) and (39e), we obtain

$$A_{w_0} w_{0,XX}^{i} + B_{w_0} p_{,XX} + C_{w_0} p - \mathscr{I}_Y(\sigma_{0_{XX}} Y) = 0.$$
 (60)

Substituting Eqs. (59), (60) and their derivatives into Eq. (58), one finds a linear fourth-order biquadratic BVP in p(X) only, that is,

$$k_4 p_{,XXXX} + k_2 p_{,XX} + k_0 p = \bar{k},$$
 (61a)

$$p(0) = 0,$$
 (61b)

$$p(l) = 0, (61c)$$

$$k_2^{\text{BC}} p_{XX}(0) + k_0^{\text{BC}} p(0) = \bar{k}^{\text{BC}},$$
 (61d)

$$k_2^{\text{BC}} p_{XX}(l) + k_0^{\text{BC}} p(l) = \bar{k}^{\text{BC}},$$
 (61e)

where we have introduced the following quantities:

$$k_4 = A_p - D_p \frac{B_{w_0}}{A_{w_0}} - F_p \frac{C_{u_0}}{A_{u_0}},$$
 (62a)

$$k_2 = B_p - D_p \frac{C_{w_0}}{A_{w_0}} - E_p \frac{B_{w_0}}{A_{w_0}} - F_p \frac{B_{u_0}}{A_{u_0}} - G_p \frac{C_{u_0}}{A_{u_0}},$$
 (62b)

$$k_0 = C_p - E_p \frac{C_{w_0}}{A_{w_0}} - G_p \frac{B_{u_0}}{A_{u_0}}, \tag{62c}$$

$$\bar{k} = -\mathscr{I}_{Y}(\sigma_{0_{XX}}Y)\frac{E_{p}}{A_{w_{0}}} + \mathscr{I}_{Y}(\sigma_{0_{XX}})\frac{G_{p}}{A_{u_{0}}} - \mathscr{I}_{Y}(\sigma_{0_{YY}}\bar{f}_{,Y}), \tag{62d}$$

$$k_2^{\text{BC}} = A_p - D_p \frac{B_{w_0}}{A_{w_0}} - F_p \frac{C_{u_0}}{A_{u_0}}, \tag{62e}$$

$$k_0^{\rm BC} = -D_p \frac{C_{w_0}}{A_{w_0}} - F_p \frac{B_{u_0}}{A_{u_0}},\tag{62f}$$

$$\bar{k}^{\rm BC} = -\mathscr{I}_{Y}(\sigma_{0_{XX}}Y)\frac{D_{p}}{A_{w_{0}}} + \mathscr{I}_{Y}(\sigma_{0_{XX}})\frac{F_{p}}{A_{u_{0}}}. \tag{62g}$$

These quantities vary with time, and they are known at each time instant from material properties and electrochemical profiles computed a-priori through matched asymptotic expansions (A).

The solution of the linear ODE in Eq. (61a) is given by the sum of the general solution of the associated homogeneous equation and a particular solution. Herein, we focus on the case in which the squares of the roots of the characteristic equation are complex conjugate, which corresponds to the parameters utilized in our simulations. In this case, given a root λ of the characteristic equation, we define $\sigma = |\text{Re}(\lambda)|$ and $\omega = |\text{Im}(\lambda)|$, where $\text{Re}(\cdot)$ and $\text{Im}(\cdot)$ are real and imaginary parts, respectively. Hence, the general solution of the ODE is given by

$$p_{G}(X) = A_{G}e^{\sigma(X-l)}\cos(\omega X) + B_{G}e^{\sigma(X-l)}\sin(\omega X) + C_{G}e^{-\sigma X}\cos(\omega X) + D_{G}e^{-\sigma X}\sin(\omega X),$$
(63)

where A_G , B_G , C_G , and D_G are determined by imposing boundary conditions in Eq. (61). It is easy to verify that the particular solution

$$p_{\mathcal{P}}(X) = \frac{\bar{k}}{k_0} \tag{64}$$

satisfies the inhomogeneous ODE in Eq. (61a). Thus, the complete solution of the ODE is given by

$$p(X) = p_{G}(X) + p_{P}(X) = A_{G}e^{\sigma(X-l)}\cos(\omega X) + B_{G}e^{\sigma(X-l)}\sin(\omega X) + C_{G}e^{-\sigma X}\cos(\omega X) + D_{G}e^{-\sigma X}\sin(\omega X) + \frac{\bar{k}}{k_{O}}.$$
(65)

By imposing the boundary conditions in Eq. (61) on the general solution in Eq. (65), we obtain the following system of equations for A_G , B_G , C_G , and D_G :

$$e^{-\sigma l}A_{\rm G} + C_{\rm G} = -\frac{\bar{k}}{k_0},$$
 (66a)

$$\cos(\omega l)A_{G} + \sin(\omega l)B_{G} + e^{-\sigma l}\cos(\omega l)C_{G} + e^{-\sigma l}\sin(\omega l)D_{G} = -\frac{\bar{k}}{k_{0}},$$
 (66b)

$$(\sigma^2 - \omega^2)e^{-\sigma l}A_{\rm G} + 2\sigma\omega e^{-\sigma l}B_{\rm G} + (\sigma^2 - \omega^2)C_{\rm G} - 2\sigma\omega D_{\rm G} = \frac{\bar{k}^{\rm BC}}{k_2^{\rm BC}}, \tag{66c}$$

$$\begin{split} &[(\sigma^2 - \omega^2)\cos(\omega l) - 2\sigma\omega\sin(\omega l)]A_{\rm G} \\ &+ [(\sigma^2 - \omega^2)\sin(\omega l) + 2\sigma\omega\cos(\omega l)]B_{\rm G} \\ &+ [(\sigma^2 - \omega^2)\cos(\omega l) + 2\sigma\omega\sin(\omega l)]C_{\rm G} \\ &+ [(\sigma^2 - \omega^2)\sin(\omega l) - 2\sigma\omega\cos(\omega l)]D_{\rm G} = \frac{\bar{k}^{\rm BC}}{k_2^{\rm BC}}. \end{split} \tag{66d}$$

Once these quantities are obtained from the linear system, we substitute them back into Eq. (65) to obtain the final expression for p(X).

Next, we compute the longitudinal displacement of the ionomer mid-axis by integrating Eq. (59) with the boundary condition in Eq. (55), such that

$$u_0^{i}(X) = -\frac{1}{A_{u_0}} \left\{ \mathscr{I}_Y(\sigma_{0_{XX}}) \left(X - \frac{l}{2} \right) + B_{u_0} \left[\mathscr{P}(X) - \mathscr{P}\left(\frac{l}{2}\right) \right] + C_{u_0} \left[p_{,X} - p_{,X} \left(\frac{l}{2}\right) \right] \right\}, \tag{67}$$

where $\mathscr{P}(X) = \int_0^X p(\tilde{X}) d\tilde{X}$. Finally, by integrating twice Eq. (60) and applying the boundary conditions in Eq. (55), we determine

$$w_0^{\mathbf{i}}(X) = \frac{1}{A_{w_0}} \left\{ \mathscr{I}_Y(\sigma_{0_{XX}}Y) \frac{X}{2}(X-l) - C_{w_0} \left[\int_0^X \mathscr{P}(\tilde{X}) \, \mathrm{d}\tilde{X} - \frac{X}{l} \int_0^l \mathscr{P}(\tilde{X}) \, \mathrm{d}\tilde{X} \right] - B_{w_0} p(X) \right\}. \tag{68}$$

By setting $\bar{f}(Y) = 0$, we obtain the following longitudinal and transverse displacements of the ionomer mid-axis for the original Euler-Bernoulli beam theory:

$$u_0^{\rm i}(X) = -\frac{1}{A_{u_0}} \mathscr{I}_Y(\sigma_{0_{XX}}) \left(X - \frac{l}{2}\right),$$
 (69a)

$$w_0^{i}(X) = \frac{1}{A_{w_0}} \mathscr{I}_Y(\sigma_{0_{XX}}Y) \frac{X}{2} (X - l). \tag{69b}$$

4.1.2 Original and enriched enhanced high-order sandwich panel theories

Despite the linearity of the original EHOSPT and enriched EHOSPT presented in Section 3.2.2, the large number of equations and couplings among the variables pose a challenge in determining a closed-form solution as we did for the enriched Euler-Bernoulli beam theory. Therefore, we pursue a different approach, by expanding the variables in a series of cosines or sines along the axial coordinate X, similar to the method of Pagano [47] to find exact plane-strain solutions in composite structures with arbitrary numbers of layers.

Specifically, we assume the following expansions for each variable:

$$u_0^i(X) = \sum_{n=1}^{\infty} U_0^{(n)} \cos\left(\frac{n\pi}{l}X\right),$$
 (70a)

$$u_1^i(X) = \sum_{n=1}^{\infty} U_1^{(n)} \cos\left(\frac{n\pi}{l}X\right),\tag{70b}$$

$$u_2^i(X) = \sum_{n=1}^{\infty} U_2^{(n)} \cos\left(\frac{n\pi}{l}X\right),\tag{70c}$$

$$u_3^i(X) = \sum_{n=1}^{\infty} U_3^{(n)} \cos\left(\frac{n\pi}{l}X\right),$$
 (70d)

$$w_0^i(X) = \sum_{n=1}^{\infty} W_0^{(n)} \sin\left(\frac{n\pi}{l}X\right),$$
 (70e)

$$w_1^i(X) = \sum_{n=1}^{\infty} W_1^{(n)} \sin\left(\frac{n\pi}{l}X\right),\tag{70f}$$

$$w_2^i(X) = \sum_{n=1}^{\infty} W_2^{(n)} \sin\left(\frac{n\pi}{l}X\right),$$
 (70g)

$$p(X) = \sum_{n=1}^{\infty} P^{(n)} \left(\frac{n\pi}{l} X \right), \tag{70h}$$

where all the variables in capital letters are Fourier coefficients that depend only on time. These expansions satisfy the essential boundary conditions in Eq. (55), such that cosines and sines are admissible functions.

Similarly, we expand the eigenstress components, constant with respect to the X coordinate, into the following series:

$$\sigma_{0_{XX}}(Y) = \sum_{n=1}^{\infty} S_{XX}^{(n)}(Y) \sin\left(\frac{n\pi}{l}X\right),\tag{71a}$$

$$\sigma_{0_{YY}}(Y) = \sum_{n=1}^{\infty} S_{YY}^{(n)}(Y) \sin\left(\frac{n\pi}{l}X\right),\tag{71b}$$

where the Fourier coefficients vary through the thickness of the ionomer, such that

$$S_{XX}^{(n)}(Y) = \begin{cases} \frac{4}{n\pi} \sigma_{0_{XX}}(Y) & \text{if n is odd,} \\ 0 & \text{if n is even,} \end{cases}$$
 (72a)

$$S_{YY}^{(n)}(Y) = \begin{cases} \frac{4}{n\pi} \sigma_{0_{XX}}(Y) & \text{if n is odd,} \\ 0 & \text{if n is even.} \end{cases}$$
 (72b)

We comment that, while the eigenstress is zero at both ends of the IPMC, natural boundary conditions would still be satisfied asymptotically [57].

By substituting the expansions in Eqs. (70) and (71) into the TPE in Eq. (46), one finds the TPE as a function of the Fourier coefficients. By setting to zero the derivative of the TPE with respect to each of these coefficients and exploiting the orthogonality of harmonic functions, we obtain the following linear system:

$$-\left(\frac{n\pi}{l}\right)A'_{u_0}U_0^{(n)} - \left(\frac{n\pi}{l}\right)B'_{u_0}U_2^{(n)} + \left[C'_{u_0} - \left(\frac{n\pi}{l}\right)^2 D'_{u_0}\right]W_1^{(n)} + \left[-\left(\frac{n\pi}{l}\right)^2 E'_{u_0} + F'_{u_0}\right]P^{(n)} + \mathscr{I}_Y\left(S_{XX}^{(n)}\right) = 0,$$
(73a)

$$\left[-\left(\frac{n\pi}{l}\right)^{2} A'_{u_{1}} + G'_{u_{1}} \right] U_{1}^{(n)} + \left[-\left(\frac{n\pi}{l}\right)^{2} B'_{u_{1}} + H'_{u_{1}} \right] U_{3}^{(n)}
+ \left[\left(\frac{n\pi}{l}\right) G'_{u_{1}} - \left(\frac{n\pi}{l}\right)^{3} I'_{u_{1}} \right] W_{0}^{(n)} + \left[\left(\frac{n\pi}{l}\right) \left(C'_{u_{1}} + D'_{u_{1}}\right) - \left(\frac{n\pi}{l}\right)^{3} J'_{u_{1}} \right] W_{2}^{(n)}
+ \left[\left(\frac{n\pi}{l}\right) \left(E'_{u_{1}} + F'_{u_{1}}\right) - \left(\frac{n\pi}{l}\right)^{3} K'_{u_{1}} \right] P^{(n)} + \left(\frac{n\pi}{l}\right) \mathscr{I}_{Y} \left(S_{XX}^{(n)} Y\right) = 0,$$
(73b)

 $+\mathscr{I}_{Y}\left(S_{YY}^{(n)}\bar{f}_{,Y}\right)=0.$

$$-\left(\frac{n\pi}{l}\right)^{2}A'_{u2}U_{0}^{(n)} + \left[-\left(\frac{n\pi}{l}\right)^{2}B'_{u_{2}} + G'_{u_{2}}\right]U_{2}^{(n)} + \left[\left(\frac{n\pi}{l}\right)(C'_{u_{2}} + D'_{u_{2}}) - \left(\frac{n\pi}{l}\right)^{3}H'_{u_{2}}\right]W_{1}^{(n)} + \left[\left(\frac{n\pi}{l}\right)(E'_{u_{2}} + F'_{u_{2}}) - \left(\frac{n\pi}{l}\right)^{3}I'_{u_{2}}\right]P^{(n)} + \left(\frac{n\pi}{l}\right)\mathcal{F}_{Y}\left(S_{XX}^{(n)}Y^{2}\right) = 0,$$

$$-\left(\frac{n\pi}{l}\right)^{2}A'_{u_{3}} + G'_{u_{3}}\right]U_{1}^{(n)} + \left[-\left(\frac{n\pi}{l}\right)^{2}B'_{u_{3}} + H'_{u_{3}}\right]U_{3}^{(n)} + \left[\left(\frac{n\pi}{l}\right)G'_{u_{3}} - \left(\frac{n\pi}{l}\right)^{3}J'_{u_{3}}\right]W_{2}^{(n)} + \left[\left(\frac{n\pi}{l}\right)(C'_{u_{3}} + D'_{u_{3}}) - \left(\frac{n\pi}{l}\right)^{3}J'_{u_{3}}\right]W_{2}^{(n)} - \left[\left(\frac{n\pi}{l}\right)(E'_{u_{3}} + F'_{u_{3}}) - \left(\frac{n\pi}{l}\right)^{3}K'_{u_{3}}\right]P^{(n)} + \left(\frac{n\pi}{l}\right)\mathcal{F}_{XX}^{(n)}Y^{3} = 0,$$

$$-\left[\left(\frac{n\pi}{l}\right)^{2}C'_{u_{0}} - E'_{u_{0}}\right]U_{1}^{(n)} + \left[\left(\frac{n\pi}{l}\right)^{2}D'_{u_{0}} - F'_{u_{0}}\right]U_{3}^{(n)} + \left[\left(\frac{n\pi}{l}\right)^{3}A'_{u_{0}} - \left(\frac{n\pi}{l}\right)E'_{u_{0}}\right]W_{0}^{(n)} + \left[\left(\frac{n\pi}{l}\right)^{3}B'_{u_{0}} - \left(\frac{n\pi}{l}\right)^{3}H'_{u_{0}}\right]W_{2}^{(n)} + \left[\left(\frac{n\pi}{l}\right)^{3}G'_{u_{0}} + \left(\frac{n\pi}{l}\right)^{3}I'_{u_{0}}\right]P^{(n)} = 0,$$

$$-\left[\left(\frac{n\pi}{l}\right)^{3}B'_{u_{0}} - \left(\frac{n\pi}{l}\right)H'_{u_{0}}\right]W_{2}^{(n)} + \left[\left(\frac{n\pi}{l}\right)^{3}C'_{u_{1}} - \left(\frac{n\pi}{l}\right)(G'_{u_{1}} + H'_{u_{1}}\right)\right]U_{2}^{(n)} + \left[\left(\frac{n\pi}{l}\right)^{3}A'_{u_{0}} - \left(\frac{n\pi}{l}\right)(I'_{u_{1}} + E'_{u_{1}}\right]P^{(n)} - \left(\frac{n\pi}{l}\right) + \mathcal{F}_{Y}\left(S_{YY}^{(n)}\right) = 0,$$

$$-\left[\left(\frac{n\pi}{l}\right)^{3}A'_{u_{1}} - \left(\frac{n\pi}{l}\right)^{2}J'_{u_{1}} + D'_{u_{1}}\right]W_{1}^{(n)} + \left[\left(\frac{n\pi}{l}\right)^{3}D'_{u_{2}} - \left(\frac{n\pi}{l}\right)(I'_{u_{2}} + J'_{u_{2}}\right)\right]U_{3}^{(n)} + \left[\left(\frac{n\pi}{l}\right)^{3}D'_{u_{2}} - \left(\frac{n\pi}{l}\right)(I'_{u_{2}} + J'_{u_{2}}\right)\right]U_{3}^{(n)} + \left[\left(\frac{n\pi}{l}\right)^{3}A'_{u_{2}} - \left(\frac{n\pi}{l}\right)(I'_{u_{2}} + J'_{u_{2}}\right)\right]U_{3}^{(n)} + \left[\left(\frac{n\pi}{l}\right)^{3}D'_{u_{2}} - \left(\frac{n\pi}{l}\right)(I'_{u_{2}} + J'_{u_{2}}\right)\right]U_{3}^{(n)} + \left[\left(\frac{n\pi}{l}\right)^{3}A'_{u_{2}} - \left(\frac{n\pi}{l}\right)(I'_{u_{2}} + I'_{u_{2}}\right)\right]W_{2}^{(n)} - \left(\frac{n\pi}{l}\right)$$

$$+ \left[\left(\frac{n\pi}{l}\right)^{3}A'_{u_{2}} - \left(\frac{n\pi}{l}\right)^{2}M'_{u_{2}} + F'_{u_{2}}\right]P^{(n)} + \left[\left(\frac{n\pi}{l}\right)^{3}B'_{u_{2}} - \left(\frac{n\pi}{l}\right)(I'_{u_{2}} + F'_{u_{2}}\right)\right]U_{3}^{(n)} + \left[\left(\frac{n\pi}{l}\right)^{3}A'_{u_{2}} - \left(\frac{n$$

This system of equations can be solved to find $U_0^{(n)}$, $U_1^{(n)}$, $U_2^{(n)}$, $U_3^{(n)}$, $W_0^{(n)}$, $W_1^{(n)}$, $W_2^{(n)}$, and $P^{(n)}$, from which one can recover $u_0^i(X)$, $u_1^i(X)$, $u_2^i(X)$, $u_3^i(X)$, $u_3^i(X)$, $w_0^i(X)$, $w_1^i(X)$, $w_2^i(X)$, and p(X) from Eq. (70). The solution of the original EHOSPT can be obtained by setting $\bar{f}(Y) = 0$ in Eq. (73).

4.2 Comparison between structural models

We examine IPMC response to a step voltage of $\bar{V}=5\,V_{\rm th}$ applied across its electrodes at time $t_0=0\,\rm s$. We focus on the steady-state profiles at $t=7.5\,\rm s$. Geometrical and physical parameters for the ionomer and electrodes are listed in Tabs. 1 and 5, respectively. Constants are selected from the literature on NafionTM [27, 29, 58] and platinum electrodes [29, 59]. Only the dielectric constant, ε , is artificially inflated, such that the ratio $\delta=\frac{\lambda}{\hbar}$ of the Debye screening length and the semi-thickness of the ionomer is equal to 10^{-3} . Although we could attempt at simulations with smaller Debye screening lengths, we choose this value to ease the visualization of the boundary layers.

In our FE simulations, we utilize the UEL implemented in ABAQUSTM to study the non-linear, bidirectionally coupled mechanics and electrochemistry of the ionomer. The UEL implements a quadrilateral quadratic element with eight nodes, with integration scheme through Gaussian quadrature [60]. In this framework, electrodes are modeled as isotropic metal layers. Consistent with our discussion in Section 2.1, we do not include any electrochemical variable in the electrodes. For the electrodes, we utilize CPE8 elements, a quadratic eight-node plane-strain element built-in in ABAQUSTM. (Dealing with finite deformations in ABAQUSTM, the linear elastic model posits that the Cauchy stress is linearly related to the logarithmic strain.) We implement a mesh of 36,000 elements, with 4,000 on the electrodes. In order to resolve the boundary layers at the interface between ionomer and electrodes, the mesh is refined on the ionomer side near the interfaces, as shown in Fig. 4. Our elasticity framework is free from numerical issues that are typical of elastic-perfectly-plastic models, such that a suitable mesh refinement is sufficient to accurately capture strain localization in the boundary layers. To facilitate numerical convergence, in FE simulations, we approximate the jump in the step as a ramp, reaching the desired value at 10⁻³ s.

Parameter	Value
e [µm]	2.3
$Y_{\rm el}$ [Pa]	168×10^{9}
$v_{ m el}$	0.39

Table 5 Electrodes' parameters utilized in the simulations.

For the solution of the original Euler-Bernoulli beam theory, we directly evaluate Eq. (69) to find $u_0^i(X)$ and $w_0^i(X)$, which completely determine the displacement field of the IPMC. With respect to the enriched Euler-Bernoulli beam theory, we find the coefficients for p(X) in Eq. (61) from the system in Eq. (66), we evaluate the integrals of p(X), and ultimately substitute them in Eqs. (67) and (68) to obtain $u_0^i(X)$ and $w_0^i(X)$, respectively. The original and enriched EHOSPT require the solution of a 7×7 and 8×8 linear system for each harmonic, respectively. To mitigate Gibbs phenomenon [61] in both of these theories, we utilize 5,000 harmonics, which we determine by solving the system in Eq. (73) for $n = 1, \ldots, 5000$. Once the Fourier coefficients for each harmonic have been computed, we find the longitudinal and transverse displacements through Eq. (70), truncated to 5,000 terms. The code implementing this procedure has been verified through the method by Batra and Liang [62], where one computes the eigenstress components and forces required to obtain a known displacement field and utilizes the code to verify the displacement.

We assess the accuracy of the four proposed structural theories against FE simulations, by considering longitudinal and transverse displacements of the mid-axis, through-

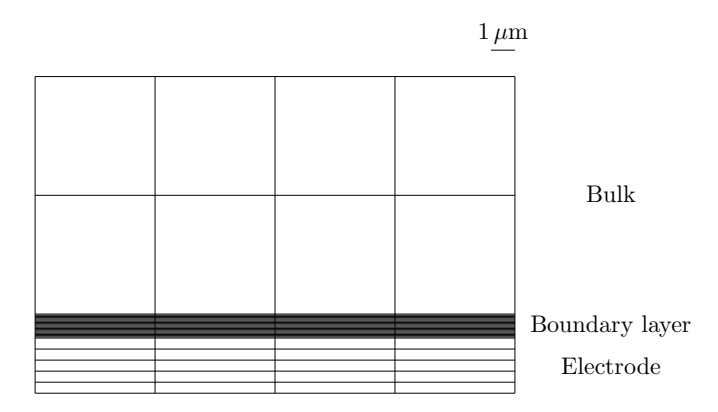


Fig. 4 Detail of the mesh near an electrode. The mesh is relatively coarse in the bulk of the ionomer, and it is highly refined at the interface with the electrode to resolve the boundary layer on the ionomer side. A relatively fine mesh is utilized to discretize the electrode.

the-thickness displacement of the mid-span section with respect to the mid-axis, longitudinal and transverse displacements of anode and cathode, and axial, through-the-thickness, and shear stresses in the ionomer. Displacements are automatically available from FE simulations. Stresses are reconstructed from Eq. (7), utilizing as infinitesimal strain tensor the nominal strain tensor available as a FE output.

First, we examine the accuracy of the four structural theories in reconstructing the macroscopic deflection of IPMCs, in terms of the displacement of the mid-axis. With respect to the longitudinal displacement of the mid-axis in Fig. 5(a), we register symmetric profiles with respect to X=l/2, as one should expect from the boundary conditions in Eq. (55). The positive slope of the displacement along the IPMC axis indicates an overall extension of the IPMC, as noted in Section 2.2 for uniform bending and zero-thickness electrodes. The original Euler-Bernoulli beam theory shows a linear profile of the mid-axis displacement along the IPMC span, similar to FE simulations, but with a different slope. The original EHOSPT displays a fifth-order polynomial trend along the IPMC length (adjusted $R^2=0.9996$), which is linear in the vicinity of the mid-span, but becomes progressively nonlinear toward the ends of the IPMC. While this structural theory provides a good estimate of the longitudinal displacement near the mid-span, the error increases as we move away from it. On the contrary, the enriched Euler-Bernoulli beam theory and EHOSPT both provide an accurate prediction of the linear profile of the longitudinal mid-axis displacement, closely matching FE simulations.

The transverse displacement of the mid-axis in Fig. 5(b) further corroborates our claim regarding the inadequacy of the original Euler-Bernoulli beam theory to study IPMC actuation. In fact, this structural theory predicts a parabolic profile (see Eq. (69)) with an opposite concavity with respect to the FE solution. Such an effect has already been observed in Boldini and Porfiri [31] for uniform bending and zero-thickness electrodes, and it is associated with the modification of the effective axial stress due to strain localization near the electrodes. The original Euler-Bernoulli beam theory does not include this correction, thereby failing to predict bending toward the cathode (that is, back-relaxation), that is observed in FE. This phenomenon is captured by the original EHOSPT, which can account for through-the-thickness deformations. However, these strains are not localized in the vicinity of the electrodes, whereby the through-the-thickness strain only varies linearly along the ionomer

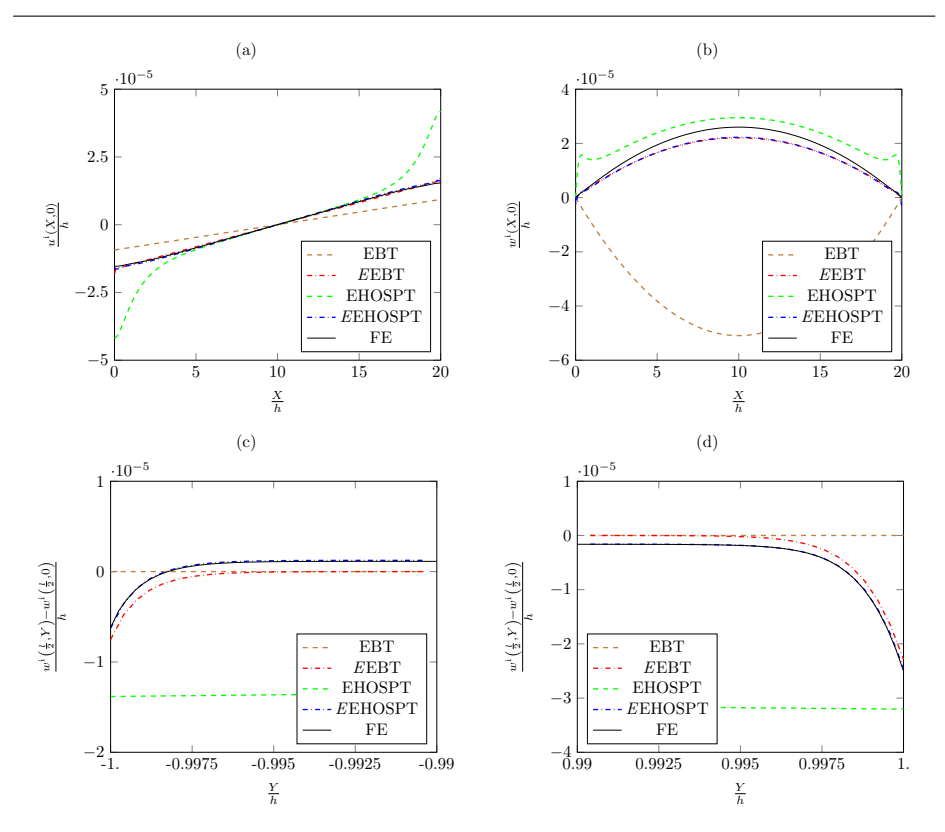


Fig. 5 Longitudinal (a) and transverse (b) displacement of the IPMC mid-axis and through-the-thickness displacement of the ionomer relative to the mid-axis, near the anode (c) and cathode (d) at the mid-span. Reported results refer to original Euler-Bernoulli beam theory (EBT, dashed brown line), enriched Euler-Bernoulli beam theory (EEBT dash dotted red line), original enhanced high-order sandwich panel theory (EHOSPT, dashed green line), enriched enhanced high-order sandwich panel theory (EEHOSPT, dash dotted blue line), and FE simulations (solid black line), at time 7.5 s. Coordinates and displacements are nondimensionalized with respect to the ionomer semi-thickness *h*.

thickness. This limitation can explain the discrepancy between the original EHOSPT and FE results, where the original EHOSPT overpredicts IPMC deflection and shows two peaks in the proximity of IPMC ends, which are absent in FE simulations. Similar to the longitudinal displacement of the mid-axis, the enriched structural theories show highly comparable results, with a slightly smaller peak displacement at the mid-span section when compared to FE.

In addition to the mid-axis displacement, we evaluate the performance of the proposed structural theories in predicting the through-the-thickness displacement of IPMC cross-sections. Toward this goal, we consider the through-the-thickness displacement of the mid-span section with respect to the mid-axis, whose profiles in the vicinity of the electrodes are shown in Fig. 5(c-d). The original Euler-Bernoulli beam theory always yields a null relative displacement, since it assumes that the transverse displacement of the ionomer is point-wise equal to that of the mid-axis, see Eq. (32b). As one should expect from Eq. (41b), the original EHOSPT shows a parabolic profile of the relative through-the-thickness displacement, which is not reminiscent of the strain localization close to the electrodes that is predicted

by FE simulations. Thus, both the original theories fail in anticipating FE results, which are characterized by two boundary layers at the ionomer-electrode interfaces. Interestingly, the enriched Euler-Bernoulli beam theory displays such a localization, but its predictions show an almost constant shift with respect to FE results within the regions in Figs. 5(c-d). The only structural theory that accurately predicts the through-the-thickness displacement relative to the mid-axis is the enriched EHOSPT, which is in close agreement with FE simulations. Compared to the enriched Euler-Bernoulli beam theory, the enriched EHOSPT accounts for the transverse deformability of the ionomer, which provides an additional parabolic deformation along the ionomer thickness that is important to capture the effect of the large contrast between the compliance of the ionomer and electrodes.

Moreover, we consider longitudinal and transverse displacements of the anode and cathode as a measure of structural theories' ability to reconstruct multiaxial deformations in IPMCs. Figure 6(a) illustrates the longitudinal displacement of the top face of the anode, that is, the top face of the IPMC. Similar to the longitudinal displacement of the mid-axis, the original Euler-Bernoulli beam theory yields a linear profile along the IPMC span, whose slope does not coincide with FE simulations. The original EHOSPT and the two enriched structural theories offer equivalent results, matching FE simulations, with the largest deviation shown by the enriched Euler-Bernoulli beam theory. From Fig. 6(b), we find that the original Euler-Bernoulli beam theory fails in estimating the deflection of the top face of the anode. The original EHOSPT provides an accurate prediction of the displacement near the mid-axis section, while it overestimates peaks close to the ends of the IPMC. The enriched Euler-Bernoulli beam theory and enriched EHOSPT closely match FE analysis along the entire IPMC span. With respect to the longitudinal displacement of the bottom face of the cathode, which corresponds to the bottom face of the IPMC, Fig. 6(c) pictures a scenario similar to the other electrode, with the original Euler-Bernoulli beam theory being unable to anticipate the correct slope and the other three structural theories offering comparable results. In this case, the enriched Euler-Bernoulli beam theory shows a lower error compared to EHOSPT-based theories. The scenario for the transverse displacement of the top face of the anode is mirrored in the transverse displacement of the bottom face of the cathode, displayed in Fig. 6(d). The error of the original Euler-Bernoulli beam theory with respect to FE simulations is larger than in the previous case, while the other three theories slightly undepredict the peak value of the deflection at the mid-span section, with additional discrepancies for the original EHOSPT near the ends of the IPMC.

Quantities associated with the derivatives of the displacement field, such as strains and stresses, are other critical metrics for testing the accuracy of structural theories. Given that our structural theories rely on a Saint-Venant approach for the electrochemistry, we do not expect to obtain accurate predictions of mechanical deformations in the vicinity of the ends of the IPMC, where edge effects may affect the electrochemistry. Thus, we focus on axial, through-the-thickness, and shear stresses at the mid-span of the IPMC. In Figs. 7(a-b), we present the axial stress in the ionomer in the vicinity of the electrodes. Both original theories cannot predict stress concentration that is identified in the FE simulations, offering compelling evidence in favor of the inclusion of the proposed enrichment. On the other hand, the results from enriched Euler-Bernoulli and enriched EHOSPT accurately follow the boundary layers predicted by FE simulations, both on the anode and cathode sides.

The results for the through-the-thickness stress, whose profile near the electrodes is shown in Figs. 7(c-d), mirror those for axial stress. Once again, original theories cannot anticipate through-the-thickness stress concentration near the electrodes, while the enriched structural theories beget an almost perfect prediction compared to FE analyses. Contrary to the case of uniform bending in which the through-the-thickness stress was point-wise

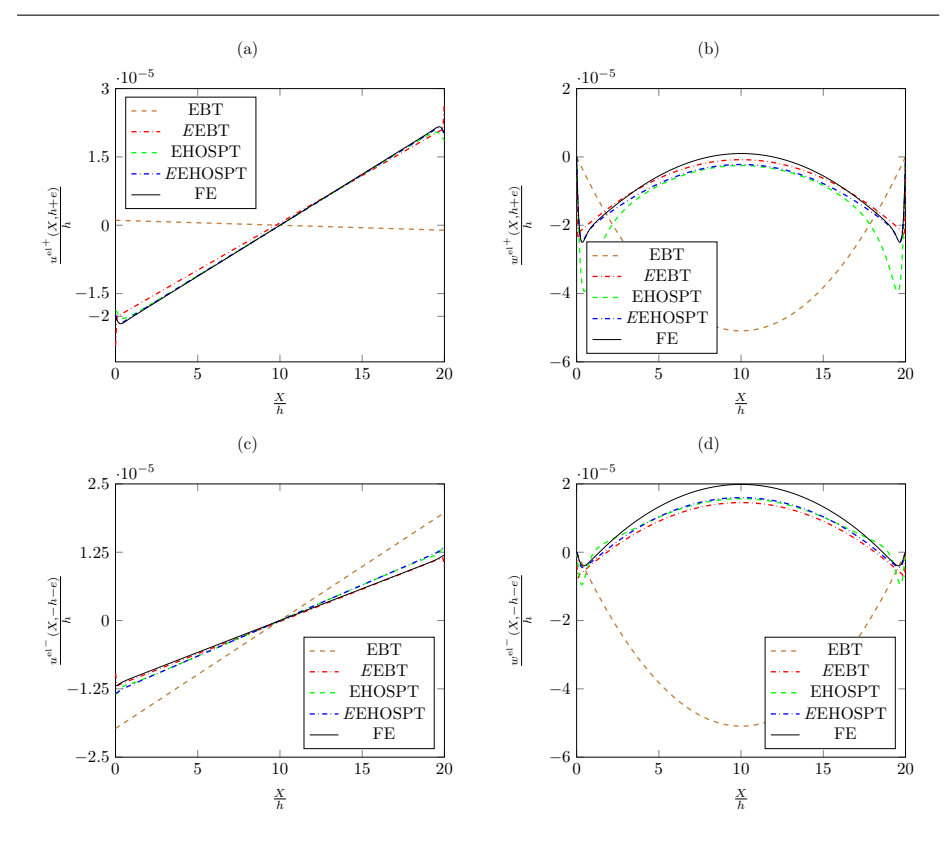


Fig. 6 Longitudinal (a, c) and transverse (b, d) displacement of the top face of the anode (a, b) and bottom face of the cathode (c, d). Reported results refer to original Euler-Bernoulli beam theory (EBT, dashed brown line), enriched Euler-Bernoulli beam theory (*E*EBT dash dotted red line), original enhanced high-order sandwich panel theory (*E*HOSPT, dashed green line), enriched enhanced high-order sandwich panel theory (*E*EHOSPT, dash dotted blue line), and FE simulations (solid black line), at time 7.5 s. Coordinates and displacements are nondimensionalized with respect to the ionomer semi-thickness *h*.

zero along the ionomer thickness (see Section 2.2), the through-the-thickness stress may dominate the axial stress, further supporting the need of considering multiaxial deformations when studying IPMC actuation.

As one should expect, shear stresses at the mid-span are much smaller than the other components of the stress tensor. Consistent with this observation, all structural theories and FE simulations display negligible values of the shear strain, as shown in the proximity of electrodes in Figs. 7(e-f). Interestingly, the enriched EHOSPT provides the largest value of the shear stress, which is still six orders of magnitude smaller than the axial and through-the-thickness stresses registered in the boundary layers, such that it can be disregarded compared to the other stress components. Within the IPMC, shear stresses are only revelant toward the ends, where our Saint Venant approach for the electrochemistry fails due to edge effects, thereby challenging an accurate reconstruction of these stress components from the proposed structural theories. Should one study more severe boundary conditions [39], it might be possible to achieve accurate prediction of shear stresses through stress recovery [37, 63], based on a Jourawski approach [64].

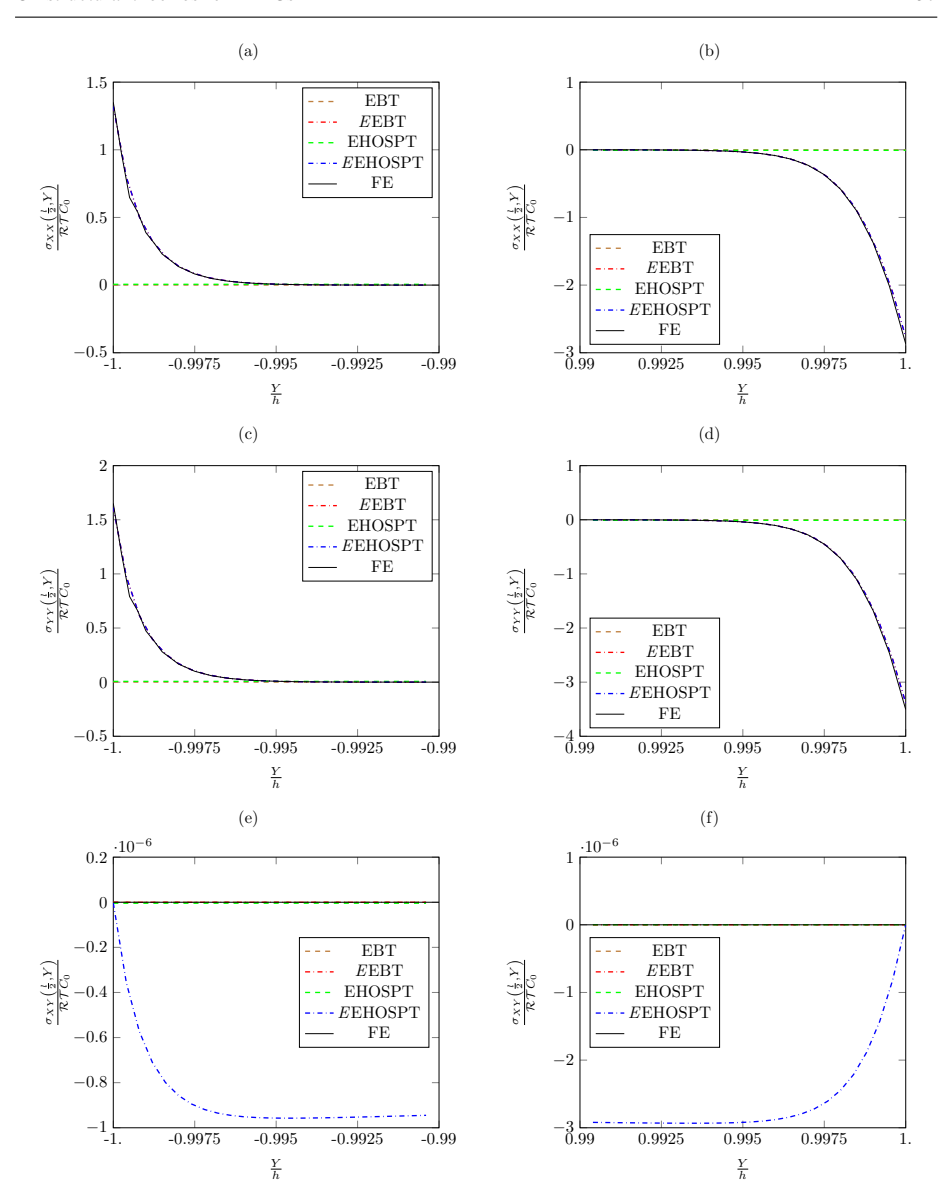


Fig. 7 Axial (a, b), through-the-thickness (c, d), and shear (e, f) stress in the ionomer, in the vicinity of the cathode (a, c, e) and of the anode (b, d, f). Reported results refer to original Euler-Bernoulli beam theory (EBT, dashed brown line), enriched Euler-Bernoulli beam theory (EEBT dash dotted red line), original enhanced high-order sandwich panel theory (EHOSPT, dashed green line), enriched enhanced high-order sandwich panel theory (EEHOSPT, dash dotted blue line), and FE simulations (solid black line), at time $7.5 \, \text{s}$. Note that EEBT profiles perfectly overlap with those of EEHOSPT in (a-d). Coordinates and stresses are nondimensionalized with respect to the ionomer semi-thickness h and reference stress \mathcal{MTC}_0 , respectively.

5 Conclusions

Ionic polymer metal composites (IPMCs) are a class of electroactive polymers that promise unprecedented applications in soft robotics [4, 5, 7] and biomedical engineering [6]. Recent advancements in the manufacturing of these materials [4] demand technical progress toward inverse design and optimization of IPMCs, where engineers could tailor the geometrical and physical properties of IPMCs to attain desired actuation. Critical to such an inverse problem is the formulation of accurate, but computationally affordable, mathematical models of IPMC actuation. The literature on IPMC actuation [16, 26, 27, 29, 41] heavily relies on traditional structural theories, such as the classical Euler-Bernoulli beam theory. However, the use of these theories and the validity of their underlying hypotheses are seldom supported by computational or experimental evidence. The presence of a complex eigenstress within the ionomer, associated with osmotic pressure and Maxwell stress, can challenge the use of these classical structural theories that are not tailored to handle the complexity of IPMC physics. Hypotheses such as the infinite rigidity of the cross-sections are unlikely to be verified in these electroactive materials.

In an effort to ascertain the validity of these claims, in Boldini and Porfiri [31] we developed a finite element (FE) environment in ABAQUSTM that implements a nonlinear continuum theory to study the mechanics and electrochemistry of IPMCs [29]. Through FE simulations, we discovered complex multiaxial deformations in the ionomer. In particular, we identified through-the-thickness strain localization in the vicinity of the ionomerelectrode interfaces, associated with the formation of boundary layers of the electrochemical variables. These through-the-thickness deformations, significantly larger than axial strains, dramatically affect the macroscopic deformation of IPMCs, thereby hampering the use of classical structural theories. While through-the-thickness deformations could reach moderate levels at the ionomer-electrode interfaces, linear elasticity predictions are generally found to be adequate. These FE analyses were complemented by a semi-analytical solution of the problem under the simplifying assumptions of uniform bending and zero-thickness electrodes. Neither the FE environment nor the developed semi-analytical solution can be leveraged for inverse design and optimization problems. FE simulations are accurate, but complex and computationally expensive, whereas the semi-analytical solution is limited to one, very specific, scenario.

Here, we tackle the problem of relaxing these two hypotheses and establish novel structural theories to accurately describe multiaxial deformations in IPMCs for non-uniform bending and electrodes with non-zero thickness. Under the assumptions of small deformations and decoupling of the electrochemistry from the mechanical deformation, we compute the counterions' concentration and voltage profiles by solving the nonlinear 1D electrochemical problem through the ionomer thickness, via the method of matched asymptotic expansions. In this way, we calculate a-priori axial and through-the-thickness eigenstress components, associated with osmotic pressure and Maxwell stress. The description of IPMC actuation is anchored in the definition of a total potential energy (TPE), which includes the strain energy of the ionomer, strain energy of the electrodes, and work done by the eigenstress. We project the kinematics of the IPMC on four different structural theories. Two of them entail classical beam theories of different complexity, namely, Euler-Bernoulli beam theory and enriched high-order sandwich panel theory (EHOSPT). The other two are enriched versions of these classical structural theories, encompassing an additional term that encodes the localized through-the-thickness deformation from uniform bending. This contraction is modulated by a function of the axial coordinate which enables the treatment of general boundary conditions that could lead to shear deformations. Balance equations for each degree of freedom are obtained from the stationarity of the TPE.

We compare the four proposed structural theories against FE simulations with inert, linear elastic electrodes. As one would expect, the original Euler-Bernoulli beam theory fails to predict any of the examined quantities, let them be displacement and stress fields. The original EHOSPT shows slightly better performance, whereby it can accurately estimate displacement and stress in the bulk of the ionomer, close to the mid-span. However, it fails to capture the ionomer displacement close to the ends of the IPMC and at the ionomer-electrode interfaces, and stress concentration in the vicinity of the electrodes. The enriched Euler-Bernoulli beam theory and enriched EHOSPT provide equivalent, accurate predictions for both displacement and stress, with the enriched EHOSPT yielding slightly better results with respect to the through-the-thickness displacement of the ionomer.

Despite the promising results of these enriched structural theories, several limitations of the present work should be addressed in future investigations. First of all, it is well known that electrodes not only play a role in determining the mechanical deformation of IPMCs, but can also affect their electrochemistry. For example, capacitance-boost associated with a rough interface between the ionomer and electrodes can be modeled through the introduction of dedicated composite layers [54]. In addition, the resistivity of electrodes may not be negligible, causing a voltage attenuation along the span of the IPMC [51]. Such variation of the voltage profile along the IPMC might trigger interesting multiaxial deformations, which can be studied by solving the through-the-thickness electrochemistry with varying applied voltage for each IPMC cross-section.

Another line of future research entails the study of thick electrodes, which can arise from repeated plating process, which is shown to improve the electrochemical properties of IPMCs, at the cost of increased bending stiffness [2, 3]. Herein, the derivation is limited to the case of thin electrodes, whereby we utilize Euler-Bernoulli beam theory to describe electrodes' mechanics. One can define an alternative structural theory to account for electrodes with larger thickness, such as Timoshenko beam theory [34, 40, 44]. Our discovery of the critical role of strain localization near the electrodes paves the way for further research on tailored physical models, such as continuum higher-order gradient models that would allow the control of the build up of deformation gradients within the boundary layers, through a material length scale [65].

Finally, this work can be extended to the study of the dynamic response of IPMCs, by including the effect of inertia forces. Interestingly, the localized through-the-thickness displacement of the enriched theories is already a function of time, thus providing an additional contribution to the inertia of the IPMC, which is associated with the electrochemistry. We should also note that the typical approach to find modes of vibration based on separation of variables [57] cannot be applied in this case, whereby the enrichment function cannot be written as the product of two independent functions of time and space.

The work presented herein provides a first, important step toward structural theories that can accurately describe multiaxial deformations of IPMCs at a reduced computational cost. The enriched Euler-Bernoulli beam theory provide fast and reliable estimations for slender IPMCs. The enriched EHOSPT can increase the accuracy of these predictions, but it calls for higher computational cost, whereby the number of field variables increases from three to eight. We expect that one should resort to the enriched EHOSPT to obtain accurate results in the case of more severe mechanical boundary conditions than those examinged in this work, for example when testing IPMCs for their blocked force where a load cell is preventing transverse displacement of a point of one of the electrodes. Overall, the proposed structural theories hold promise to unleash the full potential of novel manufacturing techniques for

IPMCs, which can benefit real-world applications and commercialization of these materials outside laboratory settings.

A Electrochemistry

Here, we put forward several hypotheses that allow us to compute a semi-analytical solution for the electrochemistry through the thickness, independently of the mechanical deformation. From the knowledge of the profiles of counterions' concentration and voltage, we can evaluate the eigenstress related to osmotic pressure in Eq. (9) and Maxwell stress in Eq. (10).

We consider a Saint-Venant solution, whereby we neglect edge effects so that the variations of the electrochemical variables along the IPMC axis and width are negligible compared to their through-the-thickness variations [29, 66]. Specifically, we suppose that the counterions' concentration and voltage depend only on the through-the-thickness coordinate Y, such that C = C(Y, t) and $\psi = \psi(Y, t)$, respectively.

Under these assumptions, the electrochemistry is described by a 1D system of two PDEs, commonly known as Poisson-Nernst-Planck (PNP) system [17, 18, 19, 50, 67]. The first equation is derived from mass conservation of the counterions in Eq. (2),

$$\frac{\partial C(Y,t)}{\partial t} + \frac{\partial J_Y(Y,t)}{\partial Y} = 0, (74)$$

where J_Y indicates the counterions' flux through the thickness of the IPMC, obtained from Eqs. (13) and (12) as

$$J_Y(Y,t) = -\mathcal{D}\left(\frac{\partial C(Y,t)}{\partial Y} + \frac{\mathcal{D}C(Y,t)}{\mathcal{R}\mathcal{T}} \frac{\partial \psi(Y,t)}{\partial Y}\right). \tag{75}$$

The second equation is the 1D Gauss law, derived from Eq. (3) as

$$\frac{\partial D(Y,t)}{\partial Y} = \mathscr{F}(C(Y,t) - C_0),\tag{76}$$

where D indicates the through-the-thickness electric displacement, which from Eq. (11) reads

$$D(Y,t) = -\varepsilon \frac{\partial \psi(Y,t)}{\partial Y}.$$
 (77)

Substituting the constitutive relations in Eqs. (75), (77) in the PDEs in Eqs. (74), (76) and assuming that material properties are homogeneous in the ionomer, we obtain the PNP system

$$\frac{\partial C(Y,t)}{\partial t} - \mathcal{D}\frac{\partial}{\partial Y}\left(\frac{\partial C(Y,t)}{\partial Y} + \frac{\mathcal{F}C(Y,t)}{\mathcal{R}\mathcal{T}}\frac{\partial \psi(Y,t)}{\partial Y}\right), \tag{78a}$$

$$-\varepsilon \frac{\partial^2 \psi(Y,t)}{\partial Y^2} = \mathscr{F}(C(Y,t) - C_0), \tag{78b}$$

which should be complemented by appropriate boundary conditions at the interface with the electrodes and initial conditions. Consistent with hypotheses in Section 2.1, we consider ion-blocking conditions at the ionomer-electrode interfaces,

$$J(-h,t) = J(h,t) = 0, (79)$$

and we assume that there is no drop of the external voltage $\bar{V}(t)$ across the electrodes, such that

$$\psi(-h,t) = -\frac{\bar{V}(t)}{2},\tag{80a}$$

$$\psi(h,t) = \frac{\bar{V}(t)}{2}.\tag{80b}$$

Furthermore, we consider the IPMC to be initially electroneutral, that is,

$$C(Y,0) = C_0,$$
 (81a)

$$\psi(Y,0) = 0. \tag{81b}$$

The system of PDEs in Eq. (78) with boundary and initial conditions in Eqs. (79), (80), and (81), represents a singularly perturbed BVP [17], due to the small value of the dielectric constant multiplying the highest order derivative in the Poisson equation in Eq. (78b). In fact, should one neglect this term, it would not be possible to satisfy both boundary conditions in Eq. (80). In this family of differential problems, boundary layers typically develop at the boundaries of the domain, challenging the application of standard numerical techniques based on the discretization of the domain, such as finite differences or FE methods [68].

The need to accurately resolve boundary layers to ensure a precise quantification of the eigenstress, along with the limitations on the aspect ratio of the elements to guarantee stability of the numerical scheme, require the use of fine meshes that drastically increase the computational burden. Specifically, the thickness of boundary layers is of the order of the so-called Debye screening length [50], which is given by

$$\lambda = \frac{1}{\mathscr{F}} \sqrt{\frac{\varepsilon \mathscr{R} \mathscr{T}}{C_0}}.$$
 (82)

For common ionomers, the Debye screening length is a few Angstrom [17], thereby hindering the feasibility of numerical simulations on millimeter- and centimeter-sized domains and calling for alternative methods to solve the problem, such as the one proposed in this paper.

Singularly perturbed problems can be solved analytically with the method of matched asymptotic expansions [32]. Specifically, we divide our computational domain into three subdomains: an "outer" region in the bulk of the ionomer, and two "inner" subdomains near the interfaces with electrodes, where we define a magnified spatial coordinate to describe the formation of boundary layers. In each of these three subdomains, we expand each variable in a power series of $\delta = \lambda/h$ quantifying the ratio of the Debye screening length and the semi-thickness of the ionomer. By considering different orders, we obtain a series of simpler systems of PDEs in each subdomain, coupled through matching conditions in the overlapping region between inner and outer subdomains, where both PDE systems should be valid. A composite solution, valid in the entire computational domain, can be assembled by summing the solutions for each subdomain and subtracting their value in the overlapping regions. A detailed solution of this mathematical problem is presented in [17].

The matched asymptotic expansion reveals that IPMC electrochemistry is determined by the solution of an RC circuit, excited by the voltage $\bar{V}(t)$ applied across the electrodes [17]. The conductivity per unit area of the resistor is given by [17]

$$\sigma = \frac{\mathscr{D}C_0\mathscr{F}^2}{2h\mathscr{R}\mathscr{T}},\tag{83}$$

while the nonlinear constitutive behavior of the capacitor, representing the charge stored in the boundary layers, is described by [17]

$$q_{S}(t) = \sqrt{\varepsilon \mathcal{RFC}_{0}} \vartheta\left(\frac{V(t)}{V_{\text{th}}}\right), \tag{84}$$

where q_S is the charge stored per unit surface of electrodes, V(t) is the voltage drop across the capacitor, and

$$\vartheta(\alpha) = \sqrt{2} \sqrt{\frac{\alpha}{\exp(\alpha) - 1} - \ln \frac{\alpha}{\exp(\alpha) - 1} - 1}.$$
 (85)

The circuit can be solved by applying Kirchhoff law, such that

$$\bar{V}(t) = V(t) + \frac{i(t)}{\sigma},\tag{86}$$

where $i(t) = dq_S(t)/dt$ is the current through the circuit.

From the solution of the ordinary differential equation (ODE) of the circuit in Eq. (86), with initially discharged capacitor (V(0) = 0), we obtain the time evolution of the voltage drop across the capacitor $\alpha(t) = V(t)/V_{th}$, which completely defines the first order composite solution through the thickness as [17]

$$C(Y, \alpha(t)) = C_0 \left[-1 + \exp\left(y^+ \left(\frac{1 - \frac{Y}{h}}{\delta}, \alpha(t)\right)\right) + \exp\left(y^- \left(\frac{1 + \frac{Y}{h}}{\delta}, \alpha(t)\right)\right) \right], \tag{87a}$$

$$\psi(Y,\alpha(t)) = \frac{\bar{V}(t)}{2} + \frac{i(t)}{2\sigma} \left(\frac{Y}{h} - 1\right) + V_{\text{th}} \left[\ln\left(\frac{\alpha(t)}{\exp\left(\alpha(t)\right) - 1}\right) - y^{+} \left(\frac{1 - \frac{Y}{h}}{\delta}, \alpha(t)\right) - y^{-} \left(\frac{1 + \frac{Y}{h}}{\delta}, \alpha(t)\right) \right], \tag{87b}$$

where $y^{\pm}(\xi^{\pm})$ are functions of the magnified variables $\xi^{\pm} = (1 \mp Y)/\delta$ near the electrodes, describing the formation and development of boundary layers. These functions are obtained by solving the following second order differential problems [17]:

$$\frac{\partial^2 y^\pm(\xi^\pm,\alpha)}{(\partial \xi^\pm)^2} = \exp(y^\pm(\xi^\pm,\alpha)) - 1, \tag{88a}$$

$$y^{+}(0,\alpha) = \ln \frac{\alpha}{\exp(\alpha) - 1}, \tag{88b}$$

$$y^{-}(0,\alpha) = \ln \frac{\alpha}{\exp(\alpha) - 1} + \alpha, \tag{88c}$$

$$\frac{\partial y^{\pm}(0,\alpha)}{\partial \xi^{\pm}} = \pm \vartheta(\alpha). \tag{88d}$$

In summary, from the solution of the circuit model we compute the voltage across the capacitor, where Eq. (86) is used, and counterions' concentration and voltage profiles through the thickness are obtained with Eqs. (87) and (88). Since these problems are independent of the deformation, the distribution of the electrochemical variables over time can be found once for all and then used to compute the eigenstress in the IPMC according to Eqs. (9) and (10).

Acknowledgements This research was supported by the National Science Foundation under Grant No. OISE-1545857.

References

- K. Oguro. Preparation procedure Ion-exchange polymer metal composites (IPMC) membranes (Retrieved on August 10, 2018). URL https://ndeaa.jpl.nasa.gov/nasa-nde/lommas/eap/IPMC_PrepProcedure.htm
- M. Shahinpoor (ed.), Ionic Polymer Metal Composites (IPMCs): Smart Multi-Functional Materials and Artificial Muscles. Smart Materials Series (Royal Society of Chemistry, 2015)
- 3. C. Jo, D. Pugal, I.K. Oh, K.J. Kim, K. Asaka, Progress in Polymer Science 38(7), 1037 (2013)
- 4. J.D. Carrico, T. Tyler, K.K. Leang, International Journal of Smart and Nano Materials 8(4), 144 (2017)
- B. Bhandari, G.Y. Lee, S.H. Ahn, International Journal of Precision Engineering and Manufacturing 13(1), 141 (2012)
- F. Carpi, E. Smela (eds.), Biomedical Applications of Electroactive Polymer Actuators (Wiley, 2009). DOI 10.1002/9780470744697
- 7. Z. Chen, Robotics and Biomimetics 4(24) (2017)
- T. Stalbaum, S. Trabia, T. Hwang, Z. Olsen, S. Nelson, Q. Shen, D.C. Lee, K.J. Kim, J. Carrico, K.K. Leang, V. Palmre, J. Nam, I. Park, R. Tiwari, D. Kim, S. Kim, in Advances in Manufacturing and Processing of Materials and Structures, ed. by Y. Bar-Cohen (CRC Press, 2018), chap. 15, pp. 379-395. URL https://www.taylorfrancis.com/books/9781315232409/chapters/10. 1201/b22020-15
- S. Trabia, Z. Olsen, K.J. Kim, Smart Materials and Structures 26(11), 115029 (2017). DOI https://doi. org/10.1088/1361-665X/aa919f
- 10. Y. Bahramzadeh, M. Shahinpoor, Soft Robotics 1(1), 38 (2014). DOI 10.1089/soro.2013.0006
- Fortuna, L., Graziani, S., La Rosa, M., Nicolosi, D., Sicurella, G., Umana, E., European Physical Journal Applied Physics 46(1), 12513 (2009). DOI 10.1051/epjap/2009019
- F. Cellini, A. Grillo, M. Porfiri, Applied Physics Letters 106(13) (2015). DOI https://doi.org/10.1063/1. 4916672
- 13. J. Kim, J.H. Jeon, H.J. Kim, H. Lim, I.K. Oh, ACS Nano 8(3), 2986 (2014). DOI 10.1021/nn500283q
- U. Johanson, A. Punning, A. Aabloo, in *Ionic Polymer Metal Composites (IPMCs): Smart Multi-Functional Materials and Artificial Muscles*, vol. 1, ed. by M. Shahinpoor (Royal Society of Chemistry, 2015), pp. 215–227. DOI http://dx.doi.org/10.1039/9781782622581
- P.G. de Gennes, K. Okumura, M. Shahinpoor, K.J. Kim, Europhysics Letters 50(4) (2000). DOI https://doi.org/10.1209/epl/i2000-00299-3
- 16. S. Nemat-Nasser, J.Y. Li, Journal of Applied Physics 87(7) (2000)
- 17. M. Porfiri, Journal of Applied Physics 104(10) (2008)

- Z. Chen, X. Tan, IEEE/ASME Transactions on Mechatronics 13(5), 519 (2008). DOI https://doi.org/10. 1109/TMECH.2008.920021
- T. Wallmersperger, D.J. Leo, C.S. Kothera, Journal of Applied Physics 101(2) (2007). DOI https://doi. org/10.1063/1.2409362
- T. Wallmersperger, B.J. Akle, D.J. Leo, B. Krplin, Composites Science and Technology 68(5), 1173 (2008). DOI https://doi.org/10.1016/j.compscitech.2007.06.001
- Z. Zhu, K. Asaka, L. Chang, K. Takagi, H. Chen, Journal of Applied Physics 114(8) (2013). DOI https://doi.org/10.1063/1.4818412
- P. Nardinocchi, M. Pezzulla, L. Placidi, Journal of Intelligent Material Systems and Structures 22(16), 1887 (2011). DOI https://doi.org/10.1177\%2F1045389X11417195
- G. Del Bufalo, L. Placidi, M. Porfiri, Smart Materials and Structures 17(4) (2008). DOI https://doi.org/ 10.1088/0964-1726/17/4/045010
- P. Leichsenring, S. Serdas, T. Wallmersperger, J. Bluhm, J. Schröder, Smart Materials and Structures 26(4), 045004 (2017)
- 25. K. Asaka, K. Oguro, Y. Nishimura, M. Mizuhata, H. Takenaka, Polymer Journal 27, 436 (1995)
- M. Shahinpoor, K.J. Kim, Smart Materials and Structures 13(6) (2004). DOI https://doi.org/10.1088/ 0964-1726/13/6/009
- 27. M. Porfiri, A. Leronni, L. Bardella, Extreme Mechanics Letters 13, 78 (2017)
- 28. M. Porfiri, H. Sharghi, P. Zhang, Journal of Applied Physics 123(014901) (2018)
- 29. Y. Cha, M. Porfiri, Journal of the Mechanics and Physics of Solids 71, 156 (2014)
- W. Hong, X. Zhao, Z. Suo, Journal of the Mechanics and Physics of Solids 58(4), 558 (2010). DOI https://doi.org/10.1016/j.jmps.2010.01.005
- A. Boldini, M. Porfiri, International Journal of Engineering Science 149, 103227 (2020). DOI https://doi.org/10.1016/j.ijengsci.2020.103227
- 32. A.H. Nayfeh, Introduction to Perturbation Techniques (Wiley, 2011)
- 33. H.G. Allen, Analysis and design of structural sandwich panels (Pergamon Press Ltd., Oxford, 1969)
- 34. D. Krajcinovic, Journal of Applied Mechanics 39(3), 773 (1972). DOI 10.1115/1.3422787
- Y.M. Ghugal, R.P. Shimpi, Journal of Reinforced Plastics and Composites 20(3), 255 (2001). DOI 10.1177/073168401772678283
- A. Tessler, M.D. Sciuva, M. Gherlone, Journal of Composite Materials 43(9), 1051 (2009). DOI 10. 1177/0021998308097730
- D. Tonelli, L. Bardella, M. Minelli, Journal of Sandwich Structures & Materials 14(6), 629 (2012). DOI 10.1177/1099636212444656
- Y. Frostig, M. Baruch, O. Vilnay, I. Sheinman, Journal of Engineering Mechanics 118(5), 1026 (1992).
 DOI 10.1061/(ASCE)0733-9399(1992)118:5(1026)
- O. Mattei, L. Bardella, European Journal of Mechanics A/Solids 58, 172 (2016). DOI https://doi.org/ 10.1016/j.euromechsol.2016.01.015
- A. Panteghini, L. Bardella, European Journal of Mechanics A/Solids 61, 393 (2017). DOI https://doi. org/10.1016/j.euromechsol.2016.10.012
- S. Lee, H.C. Park, K.J. Kim, Smart Materials and Structures 14(6), 1363 (2005). DOI 10.1088/ 0964-1726/14/6/028
- 42. L. Bardella, Journal of Mechanics of Materials and Structures 3(7), 1187 (2008). DOI http://dx.doi.org/10.2140/jomms.2008.3.1187
- C.N. Phan, Y. Frostig, G.A. Kardomateas, Journal of Applied Mechanics 79(4) (2012). DOI 10.1115/1. 4005550
- A. Leronni, L. Bardella, European Journal of Mechanics A/Solids 77, 103750 (2019). DOI https://doi.org/10.1016/j.euromechsol.2019.02.016
- 45. I.S. Sokolnikoff, Mathematical theory of elasticity, 2nd edn. (McGraw-Hill New York, 1956)
- O.A. Bauchau, J.I. Craig, Structural Analysis With Applications to Aerospace Structures (Springer, 2009). DOI 10.1007/978-90-481-2516-6
- N.J. Pagano, Journal of Composite Materials 4(1), 20 (1970). DOI https://doi.org/10.1177\ %2F002199837000400102
- B.J. Akle, D.J. Leo, Journal of Intelligent Material Systems and Structures 19(8), 905 (2008). DOI https://doi.org/10.1177/1045389X07082441
- 49. J.D. Jackson, *Classical electrodynamics*, 3rd edn. (Wiley, 1998)
- A.J. Bard, L.R. Faulkner, Electrochemical Methods Fundamentals and Applications (John Wiley & Sons. 2001)
- H. Kim, Y. Cha, M. Porfiri, Journal of Intelligent Material Systems and Structures 27(17), 24262430 (2016). DOI https://doi.org/10.1177/1045389X15620045
- 52. M. Porfiri, Physical Review E **79** (2009). DOI https://doi.org/10.1103/PhysRevE.79.041503

 M. Aureli, W. Lin, M. Porfiri, Journal of Applied Physics 105(10), 104911 (2009). DOI 10.1063/1. 3129503

- Y. Cha, M. Aureli, M. Porfiri, Journal of Applied Physics 111(12) (2012). DOI https://doi.org/10.1063/ 1.4729051
- 55. M.Z. Bazant, K. Thornton, A. Ajdari, Physical Review E 70(021506) (2004)
- 56. S. Timoshenko, J. Goodier, *Theory of Elasticity*, 3rd edn. (McGrawHill, 2001)
- 57. L. Meirovitch, Fundamentals of Vibrations, International edn. (McGraw-Hill, 2001)
- M.N. Silberstein, M.C. Boyce, Journal of Power Sources 195(17), 5692 (2010). DOI https://doi.org/10. 1016/j.jpowsour.2010.03.047
- F. Cardarelli, Materials Handbook, 3rd edn. (Springer, 2018). DOI https://doi.org/10.1007/ 978-3-319-38925-7
- T. Belytschko, W.K. Liu, B. Moran, K.I. Elkhodary, Nonlinear Finite Elements for Continua and Structures, 2nd edn. (Wiley, 2014)
- 61. P. Dyke, An Introduction to Laplace Transforms and Fourier Series, 2nd edn. (Springer-Verlag London, 2014)
- 62. R.C. Batra, X.Q. Liang, Computational Mechanics 20(5), 427 (1997). DOI 10.1007/s004660050263
- H. Matsunaga, Composite Structures 55(1), 105 (2002). DOI https://doi.org/10.1016/S0263-8223(01) 00134-9
- 64. D. Jourawski, Annales des Ponts and Chaussées 12, 328 (1856)
- S. Forest, K. Sab, Mechanics Research Communications 40, 16 (2012). DOI https://doi.org/10.1016/j. mechrescom.2011.12.002
- 66. J.A. Pelesko, D.H. Bernstein, Modeling MEMS and NEMS (CRC Press, 2002)
- Q. Shen, V. Palmre, T. Stalbaum, K.J. Kim, Journal of Applied Physics 118(12) (2015). DOI https://doi.org/10.1063/1.4931912
- A. Quarteroni, Numerical Models for Differential Problems, 2nd edn. (Springer, 2014). DOI 10.1007/ 978-88-470-5522-3